

Implicit bias as a Gauge correction: Theory and Inverse Design

Nicola Aladrah¹, Emanuele Ballarin¹, Matteo Biagetti², Alessio Ansuini², Alberto d’Onofrio¹, and Fabio Anselmi^{*1,3}

¹Università di Trieste, Dipartimento di Matematica, Informatica e Geoscienze, Trieste, Italy

²Area Science Park, Trieste, Italy

³Massachusetts Institute of Technology, Cambridge, USA

Abstract

A central problem in machine learning theory is to characterize how learning dynamics select particular solutions among the many compatible with the training objective, a phenomenon called implicit bias. This bias—emerging from the interaction between model architecture, optimization algorithm, and initialization—remain only partially characterized.

In the present work, we identify a general mechanism, in terms of an explicit geometric correction of the learning dynamics, for the emergence of implicit biases, arising from the interaction between continuous symmetries in the model’s parametrization and stochasticity in the optimization process.

Our viewpoint is constructive in two complementary directions: given model symmetries, one can derive the implicit bias they induce; conversely, one can inverse-design a wide class of different implicit biases by computing specific redundant parameterizations.

More precisely, in the diffusion-limit description of stochastic gradient descent, we show that when the dynamics is expressed in the quotient space obtained by factoring out the symmetry group of the parameterization, the resulting stochastic differential equation gains a geometric correction in the stationary distribution of the optimizer dynamics. Such correction takes the form of the log-determinant of the Gram matrix associated with the symmetry directions under orthogonality conditions.

The result yields a constructive and closed-form description of how stochastic optimization statistically favors predictors whose symmetry orbits have smaller local volume.

We compute the resulting symmetry-induced bias for a range of architectures, showing how several well-known results fit into a single unified framework. The approach also provides a practical methodology for deriving implicit biases in new settings, and it yields concrete, testable predictions that we confirm by numerical simulations on toy models trained on synthetic data, leaving more complex scenarios for future work.

Finally, we test the implicit bias inverse-design procedure in notable cases, including biases toward sparsity in linear features or in spectral properties of the model parameters.

More broadly, complementing recent thermodynamic views of symmetry in stochastic gradient descent, we interpret implicit bias as a geometric consequence of continuous parameter symmetries, arising from the induced structure of the stochastic dynamics on symmetry quotients. This perspective enables a unified and constructive framework spanning machine learning, physics, and signal processing.

*Corresponding author: fabio.anselmi@units.it

1 Introduction

1.1 Implicit bias: from norms to geometry

Modern deep neural networks (NNs) are typically trained in a strongly overparameterized regime: for a given dataset, there are surprisingly many parameter configurations that achieve zero training loss. Yet, gradient-based methods such as gradient descent (GD) and stochastic gradient descent (SGD) do not converge to one of these solutions arbitrarily. Indeed, they converge to specific parameters whose structure depends on model architecture, loss function, initialization, and optimization algorithm. This phenomenon, commonly referred to as *implicit bias* or *implicit regularization*, has been the subject of extensive theoretical and empirical investigation. Below, we provide some pointers to the vast literature on implicit bias, with no intention of covering the full topic.

The theory of implicit bias originates from the study of linear predictors trained with logistic or exponential losses on separable data [1]. In this setting, gradient descent diverges in norm but converges in direction to the hard-margin support vector machine (SVM) solution, i.e. the maximizer of the ℓ_2 margin [1, 2]. This characterization extends [3, 4] to general monotonic losses [5], non-separable data [2], and multi-class problems [6]. In all those cases, the implicit bias takes the form of a margin maximization under a suitable norm constraint, and is largely insensitive to optimization hyperparameters, assuming convergence is reached.

A second line of work analyzes implicit bias in positively homogeneous deep non-linear models. In these settings, gradient descent induces a non-Euclidean geometry on the predictor space, leading to effective low-complexity regularization akin to nuclear-norm-like penalties [7]. For deep matrix factorization and overparameterized deep networks under the square loss, gradient descent exhibits a bias towards low-rank solutions [8, 9], which is strengthened by depth and can not be explained in terms of simple norm minimization [10, 11]. These results show that the induced geometry in predictor space, rather than the loss alone, determines the actual interpolating solution that the optimizer converges to.

For shallow non-linear networks, implicit bias has been characterized in function space rather than parameter space. For wide two-layer networks and exponential-tail losses, gradient descent converges to solutions of a convex functional problem regularized by variation-type norms on measures [12]. Related work introduce path, variation, and Barron norms [13] to analyze the complexity of two-layer networks and link optimization dynamics to implicit regularization in terms of these norms [14, 15, 16]. Together, these results support the view that optimization-induced bias is central to generalization in overparameterized networks, a perspective also synthesized in recent surveys of the field [17].

At the same time, several works have highlighted the limitations of descriptions of implicit bias purely relying on norm minimization. In deep matrix factorization and completion, the solutions preferred by gradient descent cannot always be characterized in terms of fixed predictor norm minimizers [8], and there even exist settings in which implicit regularization drives all predictor norms to infinity while still promoting a low-rank structure [18]. Related studies further refine these findings by analyzing the role of large learning rates [19] and late-stage training dynamics [20]. Overall, the literature provides a diverse, architecture-dependent catalog of implicit biases, yet still *lacks a unifying geometric mechanism explaining why and how these biases arise*.

Another line of work interprets SGD as a discrete approximation of Langevin dynamics [21] and studies its continuous-time limits [22, 23]. Under small step sizes and nearly-constant noise covariance, constant-step SGD behaves like an Ornstein-Uhlenbeck process that approximately samples from

a Gibbs distribution in parameter space, around local minima [24, 25] – framing implicit bias as a stationary property of stochastic dynamics. More recently, attention has turned to SGD near manifolds of global minimizers, where anisotropic noise and non-trivial geometry shape the limiting distribution and thus the implicit bias [20, 26, 27].

The closest line of work to our perspective highlights the role of *parameter* [28, 29, 30] and optimizer [31] symmetries. Many neural architectures admit continuous or discrete reparameterization (e.g. scaling or rotations) that leave the predictor invariant, giving rise to degenerate manifolds of minimizers. Recent work analyzes SGD along such symmetry directions and shows that it converges to *noise equilibria* governed by balanced contributions from different modes [28]. Related work has interpreted discrete-time SGD from a thermodynamic perspective, identifying effective entropic corrections to the loss that arise from mini-batch noise and discretizations effects, and showing how the resulting entropy gradients generate symmetry-breaking effects that shape macroscopic learning dynamics [32]. A more detailed comparison with this line of research will be later in the paper.

Together, these results indicate that symmetry, geometry, and stochasticity are tightly coupled in implicit regularization [30], leading to a unifying view: *implicit bias has a fundamental geometric component*.

Another line of research, potentially related to our approach, studies the role of symmetry and geometry in statistical phenomena, including statistics on quotient manifolds. In [33] the author analyzes shapes as equivalence classes under Lie group actions, motivating statistical methods on manifolds and quotients, including intrinsic means [34] and GPCA [35]. Subsequent work showed that noise pushed forward through quotient maps induces systematic bias in statistical estimators due to orbit geometry and curvature [36]. In parallel, statistical physics established that imposing constraints in stochastic systems produces geometric corrections, such as the Fixman determinant in constrained Langevin dynamics [37] and related log-determinant drifts in Riemannian sampling methods [38, 39, 40].

1.2 Our viewpoint and contributions — An informal outlook

Existing work often either studies a fixed quotient space of predictors, or analyzes stochastic dynamics under externally imposed constraints. We instead show that *continuous symmetries of redundant parameterizations* induce a *geometric correction* to stochastic learning dynamics. Concretely, when one passes from the predictors statistics on the predictor space, Θ , to that on the associated quotient, $\bar{\Theta}$, the stationary law acquires a Jacobian term governed by the determinant of a symmetry-induced Gram matrix. This leads to an effective dynamics in which the correction can be interpreted as an implicit bias arising from geometric properties in the way we count solutions in predictor space. Following [30], we start from the observation that many overparameterized models exhibit a non-trivial continuous symmetry group \mathcal{G} acting smoothly on the model parameters θ . Its action partitions Θ into orbits, $\mathcal{O}_\theta = \{g \cdot \theta : g \in \mathcal{G}\}$, and all θ in the same orbit represent the same predictor. Thus, a loss L is orbit-constant: $L(g \cdot \theta) = L(\theta)$.

The main idea underlying our approach can then be informally summarized as follows:

Although SGD evolves in parameter space Θ , in the presence of continuous parameter symmetries, the induced stochastic dynamics on the quotient space $\bar{\Theta}$ acquires a geometric correction. This correction is equivalent to adding a gauge term to the loss, given by the logarithm of a symmetry-induced volume element, an implicit bias on the effective dynamics.

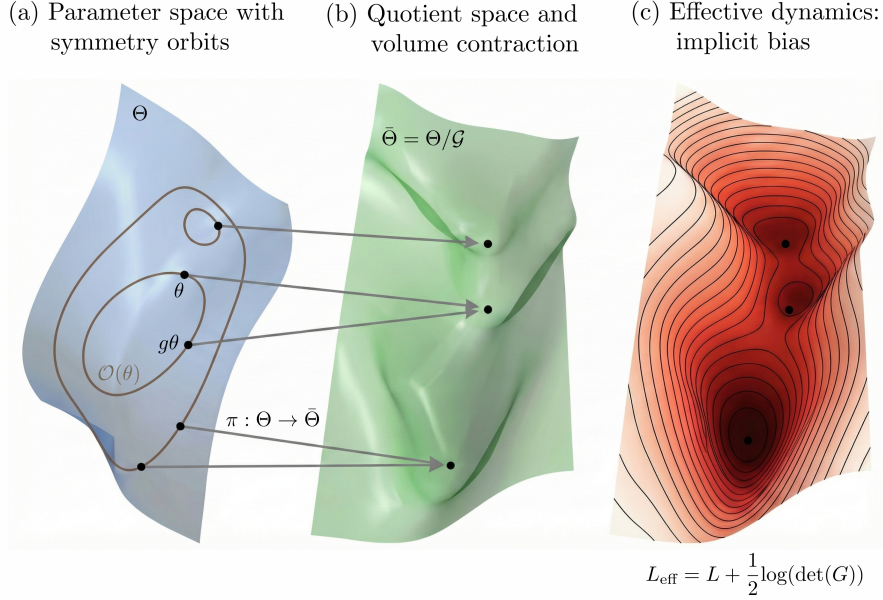


Figure 1: **Geometry of parameter symmetries and induced implicit bias.** (a) The parameter space Θ contains symmetry orbits \mathcal{O}_θ (loops) where the loss $L(\theta)$ is constant. (b) The projection onto the quotient space $\bar{\Theta}$ maps entire orbits to single points. The Jacobian of this map introduces a volume factor $\sqrt{\det G_\chi(\theta)}$. (c) This geometric correction acts as an additional potential in the effective loss L_{eff} , creating a statistical preference for solutions with smaller orbit volumes (implicit bias) without explicit regularization.

This gauge orbit-volume factor is not an algorithmic modification. It is a *characterization of which zero-loss solutions are statistically preferred once one considers predictor statistics rather than parameter statistics*.

We illustrate this geometric intuition in Figure 1. As shown, the redundancy in parameter space (Panel (a)) implies that the projection map $\pi : \Theta \rightarrow \bar{\Theta}$ induces a non-uniform measure on the quotient manifold (Panel (b)). This volume contraction results in a geometric term that effectively reshapes the optimization landscape (Panel (c)), biasing the dynamics toward regions with higher density concentrations due to smaller symmetry orbits even when the nominal loss is constant.

Paper plan In the following we first provide the mathematical details of our idea (Thm 1 and Prop 1) together with a simple *proof of concept* example (section 2). Then, we demonstrate a constructive *inverse design* principle: by engineering the symmetry structure of a parameterization, one can induce target implicit regularizers favoring sparsity on linear or spectral features of the model parameters (section 3, Props 2 and 3). Our results also provide a general theoretical framework for earlier observations on Hadamard reparameterization and sparsity [41, 42, 43, 44].

Finally, in section 4, section 5 and section 6, we explicitly compute the gauge corrections for a range of architectures trained with SGD, recovering known implicit biases and deriving new ones. Many examples are also reported in Appendix A).

In what follows we model SGD as a noisy discretizations of a stochastic differential equation (SDE) evolving on the full parameter space Θ [24, 20, 26]. All experiments, including those reported in the Appendix, are intentionally kept as simple as possible, relying on pseudorandomly-generated datasets and simple models. The analysis of more complex or state-of-the-art architectures in

task-specific scenarios is left for future work. The present contribution is intentionally scoped to the development of a novel mathematical, constructive viewpoint on implicit bias.

2 Implicit Bias as a gauge correction of SGD dynamics

2.1 Mathematical derivation

SGD as an SDE. Let us consider model parameters $\theta \in \Theta \subset \mathbb{R}^d$ and population loss $L(\theta) = \mathbb{E}[\ell(\theta; b)]$, where b encodes data or mini-batches.

One step of SGD with step size $\eta > 0$ updates parameters as

$$\theta_{k+1} = \theta_k - \eta \nabla \ell(\theta_k; b_k), \quad (1)$$

which can be decomposed into

$$\nabla \ell(\theta; b) = \nabla L(\theta) + \sigma(\theta, b), \quad \mathbb{E}[\sigma(\theta, b)] = 0, \quad \mathbb{E}[\sigma(\theta, b) \sigma(\theta, b)^\top] = \Sigma(\theta),$$

where the term $\sigma(\theta, b) \in \mathbb{R}^d$ represents the stochastic gradient noise. Under standard regularity assumptions and after time rescaling, the small-step-size limit of (1) converges in distribution to the Itô SDE [24, 20]

$$d\theta_t = -\nabla L(\theta_t) + \sqrt{\eta \Sigma(\theta)} dW_t, \quad (2)$$

where W_t is a standard Wiener process in \mathbb{R}^d .

We view (2) as a diffusion process on Θ equipped with the (state-dependent) noise metric $\Sigma(\theta)$.

Symmetry orbits and quotient space. Let Θ be a smooth manifold and \mathcal{G} a Lie group acting smoothly on it:

$$L(\rho(g, \theta)) = L(\theta) \quad \forall g \in \mathcal{G}, \forall \theta \in \Theta. \quad (3)$$

The orbit of θ is $\mathcal{O}_\theta = \{\rho(g, \theta) : g \in \mathcal{G}\} \subset \Theta$. All points on \mathcal{O}_θ represent the same predictor, hence produce the same loss.

Let \mathfrak{g} be the Lie algebra of \mathcal{G} . For $a \in \mathfrak{g}$, define the fundamental vector field

$$\xi_a(\theta) = \frac{d}{dt} \rho(e^{ta}, \theta) \Big|_{t=0}.$$

Differentiating eq. (3) yields $\nabla L(\theta)^\top \xi_a(\theta) = 0$, so the gradient is orthogonal to the vertical tangent space [45]

$$V_\theta = \text{span}\{\xi_a(\theta) : a \in \mathfrak{g}\}, \quad \nabla L(\theta) \perp V_\theta.$$

Thus the drifts act only in horizontal directions, while the motion along symmetry directions is driven by diffusion. This is also the starting point of many works studying symmetry in ML models, very recently generalized to higher order relations [46].

Theorem 1 (Gauge-fixed stationary distribution on a slice). *Let (Θ, g) be a n -dimensional smooth Riemannian manifold and let \mathcal{G} be a Lie group of dimension m acting smoothly, freely, and properly on Θ from the left.*

Assume there exists a smooth gauge-fixing map $\chi : \Theta \rightarrow \mathbb{R}^m$ such that the slice $\mathcal{S} := \chi^{-1}(0)$ is an embedded submanifold intersecting each \mathcal{G} -orbit exactly once and transversally, so that $\bar{\Theta} \simeq \mathcal{S}$.

Consider the Langevin stochastic differential equation

$$d\theta_t = -\nabla L(\theta_t) dt + \sqrt{\frac{2}{\beta}} \sigma dW_t,$$

where $L : \Theta \rightarrow \mathbb{R}$ is smooth, W_t is a standard Wiener process in \mathbb{R}^n , $\beta > 0$, the inverse temperature, and assume an effectively isotropic noise covariance $\Sigma(\theta) \approx \sigma^2 I$ with $\sigma > 0$ (see Assumption 2 in [24]). Further assume the SDE admits a stationary probability measure

$$\mu_\infty(d\theta) = Z^{-1} e^{-\frac{\beta}{\sigma^2} L(\theta)} d\text{Vol}_\Theta(\theta), \quad (4)$$

continuous with respect to the Riemannian volume $d\text{Vol}_\Theta$, where Z is a normalization constant. Define the constraint Gram matrix $G_\chi(\theta) \in \mathbb{R}^{m \times m}$ by

$$(G_\chi(\theta))_{ij} := g_\theta(\nabla \chi^i(\theta), \nabla \chi^j(\theta)). \quad (5)$$

Then the conditional (gauge-fixed) stationary measure on the slice \mathcal{S} is absolutely continuous with respect to $d\text{Vol}_\mathcal{S}$ and has density

$$\rho_{\mathcal{S}}(\theta) \propto \exp\left(-\frac{\beta}{\sigma^2} L(\theta)\right) \frac{1}{\sqrt{\det G_\chi(\theta)}}, \quad \theta \in \mathcal{S}. \quad (6)$$

Equivalently,

$$\rho_{\mathcal{S}}(\theta) \propto \exp\left(-\frac{\beta}{\sigma^2} \left(L(\theta) + \frac{\sigma^2}{2\beta} \log \det G_\chi(\theta)\right)\right), \quad \theta \in \mathcal{S}. \quad (7)$$

To define the constraint Gram matrix (Equation 5), which is the key to implicit bias formulation, we introduce the so called Faddeev-Popov matrix¹.

Faddeev-Popov matrix and orbit Gram matrix. Fix a basis $\{u_a\}_{a=1}^m$ of the Lie algebra \mathfrak{g} of \mathcal{G} , and denote by ξ_a the associated fundamental vector fields on Θ . Given a gauge-fixing map $\chi : \Theta \rightarrow \mathbb{R}^m$, we define the *Faddeev-Popov matrix* $M(\theta) \in \mathbb{R}^{m \times m}$ by

$$M_{ia}(\theta) := d\chi_\theta^i(\xi_a(\theta)) = g_\theta(\nabla \chi^i(\theta), \xi_a(\theta)), \quad (8)$$

and the *orbit Gram matrix* $H(\theta) \in \mathbb{R}^{m \times m}$ by

$$H_{ab}(\theta) := g_\theta(\xi_a(\theta), \xi_b(\theta)). \quad (9)$$

The matrix $H(\theta)$ describes the Riemannian metric induced on the symmetry orbit \mathcal{O}_θ , and therefore captures the intrinsic geometry of the redundant symmetry directions. The matrix $M(\theta)$ measures how the chosen gauge constraint χ varies along the orbit directions and thus describes the interaction between our gauge choice and the orbit geometry.

In what follows, these two matrices determine the symmetry-induced volume element appearing in the effective loss.

Proposition 1 (Constraint/orbit Gram relation). *Assume the slice $\mathcal{S} = \chi^{-1}(0)$ is orthogonal, namely for every $\theta \in \mathcal{S}$, which provides representatives that are compatible with the drift geometry of the dynamics².*

$$(T_\theta \mathcal{S})^\perp = \text{span}\{\xi_a(\theta)\}_{a=1}^m.$$

¹The Faddeev-Popov matrix and its determinant was introduced in gauge theory to handle redundancies due to continuous symmetries in functional integrals [47]. In such theories, many configurations represent the same physical state, and naive integration over all variables over-counts gauge orbits. The standard remedy is to impose a gauge condition $\chi = 0$ that intersects each orbit once and to introduce a Jacobian correcting for the change of variables. In the present approach, parameter symmetries play the role of gauge redundancies, and the Faddeev-Popov determinant appears as the Jacobian induced by conditioning the stationary distribution to a transversal slice.

²When L is G -invariant, the deterministic drift satisfies $dL_\theta(\xi_a(\theta)) = 0$ and thus $g_\theta(\nabla L(\theta), \xi_a(\theta)) = 0$ for all generators ξ_a , so $\nabla L(\theta)$ is tangent to the orthogonal complement of the orbit directions.

Fix a basis $\{u_a\}_{a=1}^m$ of \mathfrak{g} and denote by ξ_a the corresponding fundamental vector fields. Define the Faddeev-Popov matrix (8) and the orbit Gram matrix (9), then for every $\theta \in \mathcal{S}$,

$$G_\chi(\theta) = M(\theta) H(\theta)^{-1} M(\theta)^\top. \quad (10)$$

This proposition expresses the constraint Jacobian appearing in Theorem 1 in terms of orbit geometry and the Faddeev-Popov matrix, making explicit how the induced bias depends on (i) the local orbit metric H and (ii) the choice of gauge through M .

For readability, all technical proofs are deferred to Appendix E.

Summary of the mathematical reasoning When the loss is invariant under a continuous symmetry group \mathcal{G} , the stochastic dynamics evolve on a parameter space containing redundant directions: all points along an orbit represent the same predictor.

The stationary distribution of SGD is therefore naturally defined on the push-forward to the quotient space $\bar{\Theta} = \Theta/\mathcal{G}$, and gauge fixing provides an operational way to write this distribution by selecting a single representative per orbit.

Conditioning the stationary measure to a transversal slice $\mathcal{S} = \chi^{-1}(0)$ (that selects the representative of each orbit by an orthogonal intersection on the orbit) induces a Jacobian factor $(\det G_\chi)^{-1/2}$ that accounts for collapsing each orbit to a point.

While the constraint Gram matrix G_χ is defined in terms of the gauge map χ , Proposition 1 shows that, for orthogonal slices (i.e., slices whose tangent space is everywhere orthogonal to the symmetry orbits, so that motion along the slice removes only the redundant degrees of freedom), the Gauge-dependent Gramian can be expressed as $G_\chi = M H^{-1} M^\top$, where the orbit Gram matrix H encodes the intrinsic geometry of the symmetry directions and the Faddeev–Popov matrix M describes how the chosen slice intersects those directions. Different gauge choices yield different expressions of the induced density on the slice. So, the natural question is: which gauge choice makes the symmetry-induced bias interpretable in model terms and easily computable?

Gauge choice The key observation is that the *induced stationary density on the quotient is gauge invariant* which leaves the freedom to choose the most appropriate gauge.

We introduce the *balanced gauge* as a canonical choice that aligns the slice with the orbit geometry so that $M(\theta) = H(\theta)$ on \mathcal{S} , yielding $G_\chi(\theta) = H(\theta)$ and an effective correction:

$$\log \det G_\chi(\theta) = \log \det H(\theta).$$

This choice isolates the implicit bias as a *function only of the intrinsic geometry of symmetry orbits*, which, otherwise, for another choice of the gauge χ , would be a mixed term both dependent on χ and the intrinsic geometry, and thus difficult to calculate. The exact algebraic form of the minimizer depends on the model parameterization as we will see in the next sections and Appendix.

Finally, we briefly clarify the relation between our geometric quotient approach and two recent and influential works by Ziyin et al.: the noise–equilibrium framework [28] and the neural thermodynamics framework [32]. While both approaches highlight the role of symmetries in stochastic gradient descent, they differ both in scope and in the underlying principles from which implicit bias is derived.

In [28], the authors derive a fixed–point condition along symmetry directions by studying the evolution of Noether charges, leading to an equilibrium relation (Eq. (9) therein) that balances weight decay and gradient noise. This mechanism relies on a sign–balancing of expanding and

contracting directions associated with the symmetry transformation. While this provides a sharp dynamical characterization of equilibrium along symmetry orbits, it is formulated in terms of gradient forces and noise covariances, rather than as a geometric property of the quotient space. In [32], the authors adopt a thermodynamic viewpoint and derive an effective entropic correction to the loss by expanding the discrete-time SGD dynamics in learning rate and batch sampling. The resulting entropic term (Eq. (3) therein) depends explicitly on batch-averaged gradients and discretizations effects, yielding gradient-balance conditions reminiscent of thermal equipartition.

Differently, our analysis starts from the continuous-time SDE limit of SGD and leads to an intrinsic, coordinate-free correction determined solely by the geometry of the symmetry orbits. Our main result (Theorem 1) identifies the implicit bias as the logarithm of the volume element of the quotient space, independent (under proper assumptions) of learning rate, batch structure, discretizations details.

Overall, the approaches of [28, 32] and ours should be viewed as complementary: theirs emphasize dynamical and thermodynamic balances in SGD, while ours isolates a purely geometric, symmetry-induced implicit bias.

Validity regime and applicability to SGD

Our framework targets regimes where (i) the loss is invariant under a continuous symmetry group and (ii) SGD can be approximated, at the level of long-time statistics, by a stochastic differential equation. We stress that this Langevin-type description is an assumption introduced for analytical clarity, rather than an exact representation of the discrete-time algorithm.

In particular, diffusion approximations are typically motivated when the learning rate is small and the mini-batch gradient fluctuations are weak in a sense that permits a continuous-time limit. Under such conditions, one often models SGD by an SDE whose drift is the full gradient and whose diffusion term captures gradient-noise statistics, either through an explicit additive Gaussian idealization or though limit arguments applied to mini-batch gradients [24, 20]. At the same time, the SGD noise is not truly Gaussian in general, and it is not state independent. For example, the stochastic gradient equals the full gradient when the mini-batch gradient matches it, and in particular the noise can vanish at points where the full gradient vanishes.

The symmetry-based component of our analysis is insensitive to these modelling choices: the group invariance of L fixes the orbit structure and implies that the deterministic drift is orthogonal to symmetry directions. The SDE assumption is used only to obtain a tractable expression for the stationary density and the associated orbit-volume correction. For conceptual clarity here, we therefore adopt the standard isotropic assumption $\Sigma(\theta) \approx \sigma^2 I$, which isolates the geometric contribution induced by the symmetry; this should be read as a controlled simplification rather than a claim about the exact SGD covariance.

Finally, the parameterization must enforce invariance of the loss under the group action, so that $L(\theta)$ is constant along symmetry orbits and the gradient drift has no component tangent to them. Consequently, deterministic forces do not show preference for a representative along an orbit, and exploration of orbit directions is mediated by fluctuations and their interaction with orbit geometry.

2.2 A simple example and numerical validation

We illustrate the symmetry-induced geometric correction in the simplest setting where all quantities can be easily computed. Let the parameter space be

$$\Theta := \mathbb{R}^d \setminus \{0\}, \quad \omega \in \Theta, \quad r := \|\omega\|_2,$$

equipped with the Euclidean metric. Consider over-damped Langevin dynamics

$$d\omega_t = -\nabla \ell(\omega_t) dt + \sqrt{\frac{2}{\beta}} dW_t,$$

with an isotropic loss depending only on the radius,

$$\ell(\omega) = \tilde{\ell}(r), \quad \tilde{\ell}(r) = \frac{1}{2}(r-1)^2.$$

The loss is invariant under rotations $\omega \mapsto Q\omega$ with $Q \in SO(d)$. The symmetry orbits are the spheres, $\mathcal{O}_\omega = S_r^{d-1}$, and the quotient coordinate is the radius r .

Applying Theorem 1, the induced stationary density on the quotient (or equivalently on a radial gauge slice) is

$$\rho_S(r) \propto r^{d-1} e^{-\beta \tilde{\ell}(r)}. \quad (11)$$

Equivalently,

$$\rho_S(r) \propto \exp(-\beta \tilde{\ell}_{\text{eff}}(r)), \quad \tilde{\ell}_{\text{eff}}(r) = \tilde{\ell}(r) - \frac{d-1}{\beta} \log r.$$

The logarithmic term reflects the volume scaling of the symmetry orbit $\text{Vol}(S_r^{d-1}) \propto r^{d-1}$. For $d=2$, this reduces to the familiar polar-coordinate Jacobian: the orbit is a circle, $M = I_2$, $H = r^2$, $G_\chi = r^{-2}$, and $\rho_S(r) \propto r e^{-\beta \tilde{\ell}(r)}$.

Remark. No symmetry reduction is performed during simulation: the SDE is evolved in the full ambient space $\Theta = \mathbb{R}^d \setminus \{0\}$. The symmetry enters only at the level of *analysis*, when we ask for the stationary law of the symmetry-invariant coordinate $r = \pi(\omega)$ (equivalently, the push-forward $\pi_\# \mu_\infty$ of the ambient stationary measure). This is not a mere change-of-variables in the SDE, nor a reparameterization of the stochastic forcing. Rather, the correction arises because the ambient stationary measure assigns different volume to different orbits, and integrating out the orbit directions produces a non-trivial Jacobian factor in the induced density on r . In this example, the same factor can be read off either as the orbit-volume term r^{d-1} or, equivalently, via the slice formula through the constrained Gram determinant $\det G_\chi$.

Numerical validation. To experimentally validate the results derived in subsection 2.2, we simulate the over-damped Langevin dynamics induced by an isotropic radial potential and isotropic Wigner noise in $d = 10$ dimensions, for 8×10^5 time steps, and record the radial coordinate $r_t = \|\omega_t\|_2$ after an initial burn-in period. The empirical radial density is compared with two theoretical predictions: (i) the gauge-corrected law $\rho_S(r) \propto r^{d-1} e^{-\beta \tilde{\ell}(r)}$, and (ii) the naive law $\rho_{\text{naive}}(r) \propto e^{-\beta \tilde{\ell}(r)}$.

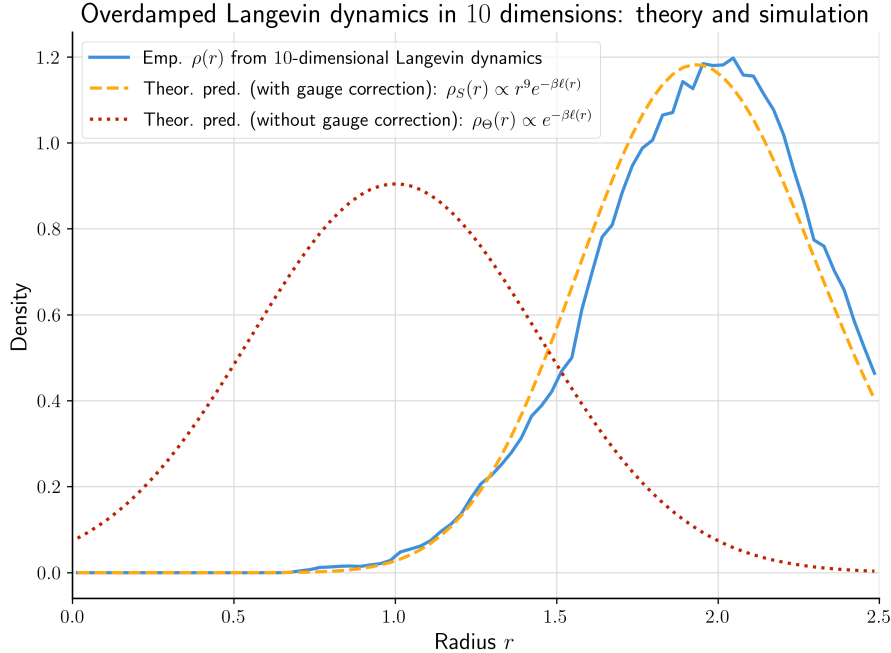


Figure 2: Empirical radial density from simulated $d = 10$ Langevin dynamics versus theoretical predictions with and without the orbit-volume (gauge) correction. The gauge-corrected prediction $\rho_S(r) \propto r^{d-1} e^{-\beta \tilde{\ell}(r)}$ matches the empirical distribution, whereas the naive prediction does not.

The result is unambiguous: the empirical distribution follows the gauge-corrected form. This confirms that, even though the dynamics are simulated entirely in the ambient space Θ , the induced stationary law of symmetry-invariant quantities $z = \pi(\omega)$ (here $z = r$) reflects the non-uniform geometry of the quotient. In particular, this example demonstrates that the gauge correction is a necessary geometric ingredient to explain the statistical preferences of dynamics under noisy optimization.

3 Inverse design of implicit bias by Symmetry engineering

The theory developed so far suggest a natural and fascinating inverse question:

Given a desired prior on the predictor (e.g. sparsity, low-rankness, group sparsity, spectral sparsity), can we construct a redundant parametrization and an associated symmetry such that the symmetry-induced implicit bias reproduces this prior?

Recent work [30] has emphasized the conceptual importance of *engineering symmetries* in models, losses, or data in order to induce structural properties. However, these approaches do not provide a principled mechanism to *reverse engineer* the symmetry so that the resulting stochastic gradient dynamics yields the prescribed geometric regularizer.

Our work provides this constructive inverse direction for a class of implicit biases. Because the symmetry-induced gauge correction is explicitly determined by the Gram matrix of the infinitesimal symmetry generators, symmetry engineering becomes a well-posed design task: one may choose a parameterization that is invariant by the action of a symmetry group \mathcal{G} so that the resulting gauge correction induces a desired implicit bias on the predictor.

We also note that our results provide a general theoretical framework for earlier observations on Hadamard reparameterizations, clarifying how their sparsity-inducing behavior arises as an implicit bias generated by symmetry-induced geometric corrections in the learning dynamics [41, 42, 43, 44].

3.1 Constructive inverse design of implicit biases via scalar factorizations

Here we consider the simple symmetry associated to a factorization of the type $z = uv$, $z, u, v \in \mathbb{R}$. We show that it is enough to induce a class of *logarithmic sparsity-promoting implicit biases* on target linear features of the predictors:

$$L_{\text{IB}}(w) = \sum_i \log|(Aw)_i|, \quad (12)$$

where A is a linear operator. In the small-noise limit, the logarithmic singularity at $(Aw)_i = 0$ strongly suppresses small but non-zero coefficients, resulting in an effective ℓ_1 -type sparsity. The role of A is to define the type of features to be sparsified. For instance, as we will see, if we want coordinate sparsity we choose $A = I$. For total variation, $A = \nabla$

We now describe in detail how, starting from Theorem 1 and Proposition 1, we can derive eq. (12).

Given a desired bias of the form (12), we first identify the linear features we want to sparsify, choosing the linear operator A

$$z = Aw \in \mathbb{R}^m, \quad z_i = (Aw)_i.$$

The inverse-design construction acts on these transformed coordinates, i.e. the learning happens on $w = A^{-1}z$. Linearity of A is essential (see section 3.2): it ensures that the zero-loss manifold remains affine in predictor space and that the geometric reduction along symmetry orbits is well defined. For each feature z_i , we introduce a two-factor redundant parameterization

$$z_i = u_i v_i, \quad (u_i, v_i) \in \mathbb{R}^2. \quad (13)$$

This choice leads to the coordinate-wise scale symmetry

$$(u_i, v_i) \mapsto (\lambda_i u_i, \lambda_i^{-1} v_i), \quad \lambda_i > 0, \quad (14)$$

independently for each i . parameterizing the symmetry action as $\lambda_i = e^{t_i}$ and expanding to first order in t_i yields

$$u_i \mapsto u_i + t_i u_i + O(t_i^2), \quad v_i \mapsto v_i - t_i v_i + O(t_i^2).$$

The fundamental vector field along the i -th symmetry direction is therefore

$$X_i = \frac{d}{dt_i} \Big|_{t_i=0} (u, v) = (u_i, -v_i).$$

Equipping parameter space with the Euclidean metric, the symmetry Gram matrix is obtained by taking inner products of these tangent vectors. Being the symmetry coordinate-wise, each X_i has support only on the (u_i, v_i) coordinates and the Gram matrix is diagonal with

$$(G_\chi)_{ii} = \langle X_i, X_i \rangle = u_i^2 + v_i^2.$$

Using the result of Theorem 1 the gauge geometric correction induced by stochastic gradient noise takes the form

$$L_{\text{gauge}}(u, v) = \frac{\sigma^2}{2\beta} \sum_i \log(u_i^2 + v_i^2). \quad (15)$$

To obtain the effective implicit bias in predictor space, we minimize (15) along the symmetry orbits at fixed invariant $z_i = u_i v_i$. Thus, being the *log* function monotonic, the minimization of L_{gauge} is equivalent to

$$\min_{u_i v_i = z_i} (u_i^2 + v_i^2).$$

This constrained minimization can be solved explicitly, for instance by introducing a Lagrange multiplier enforcing $u_i v_i = z_i$, and yields to the balanced solution $|u_i| = |v_i|$. Substituting back into (15), the reduced gauge correction becomes

$$L_{\text{gauge}}^{\text{red}}(w) \propto \sum_i \log |z_i| = \sum_i \log |(Aw)_i|, \quad (16)$$

up to additive constants.

Summarizing:

Proposition 2 (Scalar factorization induces logarithmic features sparsity). *Let $A : \mathbb{R}^d \rightarrow \mathbb{R}^m$ be a fixed linear operator and define linear features $z = Aw$. Consider the redundant scalar factorization*

$$z_i = u_i v_i, \quad (u_i, v_i) \in \mathbb{R}^2,$$

endowed with the coordinate-wise scale symmetry

$$(u_i, v_i) \mapsto (\lambda_i u_i, \lambda_i^{-1} v_i), \quad \lambda_i > 0.$$

Equip parameter space with the Euclidean metric and assume isotropic stochastic gradient noise with variance σ^2 .

Then, in the small-noise limit, symmetry reduction along the gauge orbits at fixed invariant z_i yields an effective implicit bias in predictor space of the form

$$L_{\text{IB}}(w) \propto \sum_{i=1}^m \log |(Aw)_i|,$$

up to additive constants independent of w .

Equivalently, the symmetry-induced geometric correction suppresses small but non-zero values of the linear features $z_i = (Aw)_i$, producing a logarithmic sparsity-promoting bias whose structure is entirely determined by the choice of the linear operator A .

3.2 Constructive inverse design via matrix factorization

We now extend the results to *non-Abelian* symmetries. While Abelian redundancies act on scalar features and yield coordinate-wise balance together with logarithmic sparsity, non-Abelian redundancies act on *matrix- or tensor-valued linear features* and induce implicit biases enforcing *spectral sparsity*. balance in this setting is no longer defined entry-wise, but emerges as the requirement that symmetry-coupled factors have isotropic covariances.

The non-Abelian analogue of (12) is an implicit bias acting on spectral invariants of a linear feature map,

$$L_{\text{IB}}(w) = \sum_j \log \sigma_j(\mathcal{A}(w)), \quad (17)$$

where $\mathcal{A}(w)$ is a linear map and $\sigma_j(\cdot)$ denotes its singular values. As in the Abelian case, this logarithmic bias acts as an effective ℓ_1 -type penalty on the spectrum in the low-noise limit.

The construction starts, as before, by selecting a linear feature map

$$Z = \mathcal{A}(w), \quad Z \in \mathbb{R}^{m \times n} \quad (\text{or higher-order tensor}),$$

which extracts the structure to be regularized. For example \mathcal{A} can be a map to a matrix or a tensor. As we required in the previous subsection, linearity of \mathcal{A} ensures that the zero-loss manifold remains affine and that symmetry reduction is well defined (see section 3.2).

Similar to the previous case we introduce a redundant factorization

$$Z = UV^\top, \quad U \in \mathbb{R}^{m \times r}, \quad V \in \mathbb{R}^{n \times r}, \quad (18)$$

together with its non-Abelian gauge symmetry

$$(U, V) \mapsto (UA, VA^{-\top}), \quad (19)$$

Let $A(t) = \exp(tX)$ with $X \in \mathfrak{gl}(r)$. By expanding,

$$A(t) = I + tX + O(t^2), \quad A(t)^{-\top} = (A(t)^{-1})^\top = I - tX + O(t^2),$$

we obtain

$$U(t) = U A(t) = U + tUX + O(t^2), \quad V(t) = V A(t) = V - tVX^\top + O(t^2).$$

Thus the fundamental vector field at (U, V) associated with X is

$$\xi_X(U, V) = (UX, -VX^\top).$$

We equip parameter space $\mathbb{R}^{m \times r} \times \mathbb{R}^{n \times r}$ with the Euclidean (Frobenius) metric

$$\langle (\Delta U, \Delta V), (\Delta U', \Delta V') \rangle = \text{tr}(\Delta U^\top \Delta U') + \text{tr}(\Delta V^\top \Delta V').$$

The orbit quadratic form at generator X is then

$$G(X, X) := \langle \xi_X, \xi_X \rangle = \|UX\|_F^2 + \|VX^\top\|_F^2 = \text{tr}(X^\top (U^\top U) X) + \text{tr}(X (V^\top V) X^\top).$$

Introduce the (positive definite) Gram matrices

$$A := U^\top U \in \mathbb{R}^{r \times r}, \quad B := V^\top V \in \mathbb{R}^{r \times r}.$$

hence

$$G_\chi(X, X) = \text{tr}(X^\top A X) + \text{tr}(X B X^\top). \quad (20)$$

Diagonal form at a balanced representative. Fix $Z = UV^\top$ and write its compact SVD

$$Z = P \Sigma Q^\top, \quad P \in \mathbb{R}^{m \times r}, \quad Q \in \mathbb{R}^{n \times r}, \quad \Sigma = \text{diag}(\sigma_1, \dots, \sigma_r), \quad \sigma_i > 0.$$

Among all factorizations $UV^\top = Z$, the Frobenius-minimal ones satisfy

$$U^* = P \Sigma^{1/2} O, \quad V^* = Q \Sigma^{1/2} O, \quad O \in O(r),$$

and at such a balanced representative we have

$$(U^*)^\top U^* = O^\top \Sigma O, \quad (V^*)^\top V^* = O^\top \Sigma O.$$

Substituting into (20) gives

$$G_\chi(X, X) = \text{tr}(X^\top \Sigma X) + \text{tr}(X \Sigma X^\top).$$

We can expand this expression entrywise. Write $X = (X_{ij})_{i,j=1}^r$ and $\Sigma = \text{diag}(\sigma_1, \dots, \sigma_r)$.

First trace.

$$(X^\top \Sigma X)_{jj} = \sum_{i=1}^r (X^\top)_{ji} (\Sigma X)_{ij} = \sum_{i=1}^r X_{ij} (\Sigma_{ii} X_{ij}) = \sum_{i=1}^r \sigma_i X_{ij}^2.$$

Summing over j gives

$$\text{tr}(X^\top \Sigma X) = \sum_{i=1}^r \sigma_i \sum_{j=1}^r X_{ij}^2.$$

Second trace.

$$(X \Sigma X^\top)_{ii} = \sum_{j=1}^r (X \Sigma)_{ij} (X^\top)_{ji} = \sum_{j=1}^r (X_{ij} \Sigma_{jj}) X_{ij} = \sum_{j=1}^r \sigma_j X_{ij}^2.$$

Summing over i gives

$$\text{tr}(X \Sigma X^\top) = \sum_{i=1}^r \sum_{j=1}^r \sigma_j X_{ij}^2 = \sum_{j=1}^r \sigma_j \sum_{i=1}^r X_{ij}^2.$$

The fully expanded diagonal-basis equation is

$$G_\chi(X, X) = \sum_{i=1}^r \sum_{j=1}^r (\sigma_i + \sigma_j) X_{ij}^2. \quad (21)$$

Determinant on the full algebra. In the same basis, the matrices E_{ij} (with a 1 in entry (i, j) and 0 elsewhere) form an orthonormal basis of $\mathbb{R}^{r \times r}$. Plugging $X = E_{ij}$ into (21) gives

$$G_\chi(E_{ij}, E_{ij}) = \sigma_i + \sigma_j.$$

Therefore the determinant on the full generator space $\mathfrak{gl}(r)$ is

$$\det G_\chi = \prod_{i=1}^r \prod_{j=1}^r (\sigma_i + \sigma_j). \quad (22)$$

Taking logs,

$$\log \det G_\chi = \sum_{i=1}^r \sum_{j=1}^r \log(\sigma_i + \sigma_j). \quad (23)$$

This is a spectral penalty. In particular, the diagonal terms $i = j$ contribute

$$\sum_{i=1}^r \log(2\sigma_i) = r \log 2 + \sum_{i=1}^r \log \sigma_i,$$

so $\sum_i \log \sigma_i$ always appears as an explicit component of the full non-Abelian log-determinant, with additional coupling terms coming from $i \neq j$.

Full $\mathrm{GL}(r)$ gauge with no finite minimizer. Suppose Z has rank $r \geq 2$, so its compact SVD is

$$Z = P\Sigma Q^\top, \quad \Sigma = \mathrm{diag}(\sigma_1, \dots, \sigma_r), \quad \sigma_1, \sigma_2 > 0.$$

All factorizations $UV^\top = Z$ can be parameterized by $R \in \mathrm{GL}(r)$ as

$$U = P\Sigma^{1/2}R, \quad V = Q\Sigma^{1/2}R^{-\top}.$$

Define the Gram matrices

$$A := U^\top U = R^\top \Sigma R, \quad B := V^\top V = R^{-1} \Sigma R^{-\top}.$$

We can arrive to a similar expression such as (22),

$$\det G_\chi = \prod_{i=1}^r \prod_{j=1}^r (a_i + b_j).$$

Now choose a one-parameter family inside $\mathrm{GL}(r)$,

$$R_\gamma := \mathrm{diag}(\gamma, 1/\gamma, 1, \dots, 1), \quad \gamma > 0.$$

Because Σ is diagonal, we can compute $A_\gamma := R_\gamma^\top \Sigma R_\gamma$ and $B_\gamma := R_\gamma^{-1} \Sigma R_\gamma^{-\top}$ entrywise:

$$A_\gamma = \mathrm{diag}(\sigma_1 \gamma^2, \sigma_2 \gamma^{-2}, \sigma_3, \dots, \sigma_r), \quad B_\gamma = \mathrm{diag}(\sigma_1 \gamma^{-2}, \sigma_2 \gamma^2, \sigma_3, \dots, \sigma_r).$$

So $a_1(\gamma) = \sigma_1 \gamma^2$ and $b_2(\gamma) = \sigma_2 \gamma^2$, and the eigenvalue corresponding to $(i, j) = (1, 2)$ is

$$\lambda_{12}(\gamma) = a_1(\gamma) + b_2(\gamma) = \sigma_1 \gamma^2 + \sigma_2 \gamma^2 = (\sigma_1 + \sigma_2) \gamma^2 \xrightarrow[\gamma \rightarrow 0]{} 0.$$

All other eigenvalues remain nonnegative, so

$$0 < \det G_\chi = \prod_{i,j} (a_i(\gamma) + b_j(\gamma)) \xrightarrow[\gamma \rightarrow 0]{} 0.$$

This shows that $\inf_{R \in \mathrm{GL}(r)} \det G_\chi = 0$ for rank $r \geq 2$. Since G_χ is positive definite for every finite $R \in \mathrm{GL}(r)$, we have $\det G_\chi > 0$ for all such R , so the infimum 0 is not attained by any finite R . Equivalently, the gauge term proportional to $\log \det G_\chi$ can be driven to $-\infty$ along a sequence R_s that approaches the boundary of $\mathrm{GL}(r)$ (where R_γ becomes singular), so there is no finite minimizer inside $\mathrm{GL}(r)$.

Restriction to a commuting subalgebra. If one restricts the generator space to the diagonal subspace

$$\mathfrak{t} := \{X = \mathrm{diag}(x_1, \dots, x_r)\},$$

then $X_{ij} = 0$ for $i \neq j$ and (21) reduces to

$$G(X, X) = \sum_{i=1}^r (2\sigma_i) x_i^2.$$

On this restricted subspace, the corresponding determinant is proportional to $\prod_i \sigma_i$, and the induced log-determinant contribution is proportional to

$$\sum_{i=1}^r \log \sigma_i,$$

up to additive constants independent of (U, V) (and hence independent of w through $Z = \mathcal{A}(w)$). and the minimum value is

$$\|U^*\|_F^2 + \|V^*\|_F^2 = 2 \operatorname{tr}(\Sigma) = 2 \sum_{i=1}^r \sigma_i(Z) = 2\|Z\|_*,$$

where $\|\cdot\|_*$ denotes the nuclear norm.

Substituting back into the gauge correction yields the reduced penalty

$$L_{\text{gauge}}^{\text{red}}(w) \propto \sum_j \log \sigma_j(Z),$$

In contrast to the Abelian case, where isotropy reduces to coordinate-wise sparseness, here it enforces *spectral sparseness* i.e. promoting low-rankness.

The restriction to a commuting (diagonalizable) subalgebra is not a loss of generality for the class of implicit biases we aim to characterize but a structural necessity to obtain a finite and well-defined geometric correction (see Paragraph 3.2).

Remark If one replaces $z = A(w)$ by a non-linear map $z = \varphi(w)$, the same reduction produces $\sum_i \log |\varphi_i(w)|$, but the induced predictor-space density generally acquires additional Jacobian-type geometric terms depending on $D\varphi(w)$. We restrict to linear A to avoid these extra contributions and to keep the interpolation sets affine. Future work will explore this research direction possibly leading to a broader class of IBs.

Summarizing:

Proposition 3 (Matrix factorization induces logarithmic spectral sparsity and norm balancing). *Let $\mathcal{A} : \mathbb{R}^d \rightarrow \mathbb{R}^{m \times n}$ be a fixed linear feature map and define*

$$Z = \mathcal{A}(w).$$

Consider the redundant matrix factorization

$$Z = UV^\top, \quad U \in \mathbb{R}^{m \times r}, V \in \mathbb{R}^{n \times r},$$

endowed with the non-Abelian gauge symmetry

$$(U, V) \mapsto (UA, VA^{-\top}), \quad A \in \mathcal{G} \subseteq \operatorname{GL}(r),$$

where \mathcal{G} is a compact Lie group, and equip parameter space with the Euclidean metric. Assume isotropic stochastic gradient noise with variance σ^2 .

Then, in the small-noise limit, symmetry reduction along the gauge orbits at fixed invariant Z selects balanced factorizations minimizing $\|U\|_F^2 + \|V\|_F^2$. Writing the compact singular value decomposition $Z = P\Sigma Q^\top$, with singular values $\{\sigma_j(Z)\}_{j=1}^r$, the reduced gauge correction induces an effective implicit bias in predictor space of the form

$$L_{\text{IB}}(w) \propto \sum_{j=1}^r \log \sigma_j(\mathcal{A}(w)),$$

up to additive constants independent of w .

Equivalently, the symmetry-induced geometric correction promotes spectral sparsity of the linear

features $\mathcal{A}(w)$, favouring low-rank structure. At equilibrium, the symmetry-coupled factors are balanced in the sense that

$$U^\top U = V^\top V,$$

or, equivalently, each singular direction carries equal norm in the two factors.

As a concluding remark of the propositions' results we note that the choice of the operators A and \mathcal{A} and the factorizations is very flexible. Admissible choices include linear combination of differential operators (e.g. Laplacian), fixed convolution operators, integral operators with prescribed kernels, linear projection, group algebras, to mention some. Moreover the results can be adapted to other type of factorizations including e.g. singular value, LU, Cholesky, QR decompositions, Khatri-Rao products, tensor products, direction/magnitude, amplitude/phase or more in general multi-linear operators. For all these cases we have a ready-to-run machinery to calculate the associated IB.

4 Numerical examples for scalar and matrix factorization IB inverse design

We now provide numerical simulations to test the theoretical predictions offered in subsection 3.1 and subsection 3.2. As already mentioned, all the simulations are intentionally kept as simple as possible.

4.1 Scalar factorization IB

Inverse-designed spectral sparsity To start off, we illustrate how to constructively engineer a bias toward *frequency-sparse* solutions in a regressor to be trained on periodic signal reconstruction.

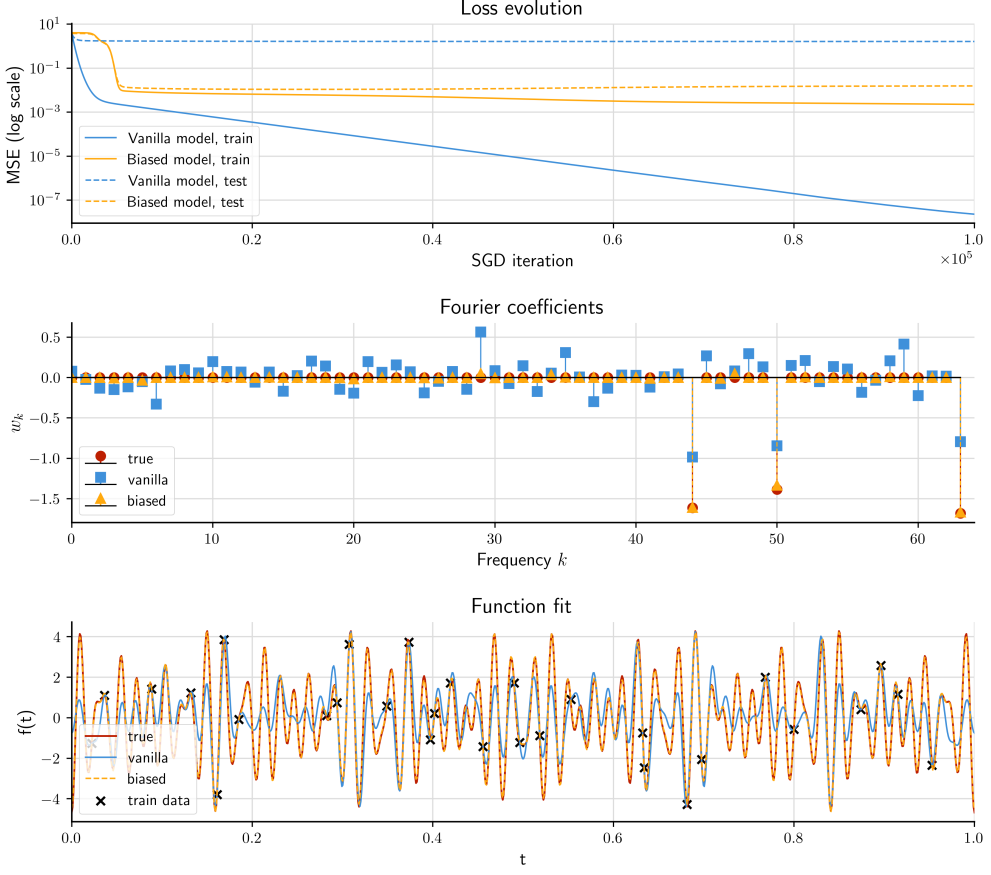


Figure 3: **Top** As training progresses, the non-biased model fails to achieve significant improvement in its loss over the test-set, while its training loss sharply decreases – a clean signal of overfitting. The biased model instead experiences a steady improvement in both losses, with its test loss soon overcoming that of the vanilla model – thus attaining far better generalization. **Middle** Recovered Fourier coefficients. Even though spectral components of the *vanilla* model partially identify the dominant modes from ground truth, their expression is insufficient and significant spectral noise is present. The biased model closely adheres to the spectral content of the ground truth. **Bottom** Analysis of the fit in time domain reveals that the *vanilla* model operates in purely-interpolating regime across training data, i.e. essentially matching the ground truth only on the training dataset and nowhere else. On the other hand, a close match between the biased model and ground truth is achieved almost everywhere. The comparison of the ℓ_1 spectral norms across the biased model (4.89), the *vanilla* model (10.72), and ground truth (4.68) corroborate the theoretical prediction of a spectral sparsification implicit bias even in the lack of explicit regularization.

This corresponds to the $A = I$ case described in subsection 3.1, where learnable parameters belong to frequency space, and we are interested in directly sparsifying Fourier coefficients. To such avail, we consider a one-dimensional time-varying signal over $t \in [0, 1]$, whose value is described in a cosine Fourier basis of dimension $D = 64$. We construct the ‘true’ frequency vector $w_{\text{true}} \in \mathbb{R}^D$ with only three non-zero coefficients at randomly chosen positive frequencies, corresponding to the resulting frequency-sparse signal $f_{\text{true}}(t) = \sum_{k=0}^{D-1} w_{\text{true},k} \cos(2\pi kt)$. We then draw uniformly at random $N_{\text{train}} = 30$ input samples, and further corrupt the corresponding outputs with additive Gaussian noise (variance 0.01). Such setup leads to a difficult and possibly under-determined problem of learning from noisy data. A large, independent test set of 2000 non-noisy samples is used to assess generalization as t varies over its domain.

We compare on the learning task two linear models trained by SGD on the mean square error loss, with no explicit regularization: (i) a *naive* cosine model that directly learns the Fourier weights $w \in \mathbb{R}^D$, and (ii) our *pq-factorized* model with parameters $(p, q) \in \mathbb{R}^D$ such that the effective Fourier coefficients factorize as $w = p \odot q$.

As the result of the training, both models achieve relatively low training MSE after convergence, adequately fitting training data. However, their Fourier spectra differ dramatically. As predicted, the *pq* model learns a solution with a much smaller Fourier ℓ_1 norm and far fewer spectral components, closely matching the ground truth. In contrast, the naive model reconstructs the training signal mostly by interpolation, making use of many small high-frequency modes that generalize poorly. Figure 3 shows the train/test loss curves for both models, the recovered spectra compared to w_{true} , and the learned signal function over a dense grid. The *pq* model clearly isolates the true low-frequency components while spontaneously suppressing spurious high-frequency modes as a result of the reverse-engineered implicit bias.

Inverse design of total variation minimization bias. Total variation (TV) regularization is a canonical prior for piecewise-constant signals and edge-preserving reconstruction, where it is typically enforced through explicit penalization or constrained optimization. Here, we demonstrate that TV reduction can be instead induced implicitly by a parameterization with an appropriate symmetry structure, as from Theorem 1, with the choice of linear operator $A = \nabla$. Figure 4 illustrates the effect of inverse-designed scalar TV implicit regularization on a simple one-dimensional signal reconstruction task, by comparing the reconstruction obtained from a non-regularized model with that produced by model inverse-designed to express a TV-minimizing implicit bias.

To assess the models experimentally, a ground-truth signal $\omega^* \in \mathbb{R}^d$ is generated as a synthetic piecewise-constant vector of size $d = 200$, with 3 jump discontinuities (leading to 4 locally-constant intervals), and therefore small total variation. Measurements are generated according to the underdetermined linear model $y^* = Q\omega^* + \varepsilon$, where $Q \in \mathbb{R}^{m \times d}$ is a randomly-sampled sensing matrix with $m = 60 \ll d$ (multivariate standard normal with diagonal covariance; variance element: $1/m$), and ε is additive Gaussian noise (variance: 0.025). Models are optimized by SGD to recover the vector $\omega \in \mathbb{R}^d$ that reproduces measurements y^* through Q .

In the baseline model, ω is directly optimized a collection of learnable scalars. In the inverse-designed model, ω is implicitly parameterized as $\nabla\omega = p \odot q$, leading to the explicit parameterization $\omega = C(p \odot q)$. There, C is the cumulative-sum operator (the discrete-inverse of the gradient operator), and $p, q \in \mathbb{R}^d$ are the actual trainable parameters.

As shown in Figure 4 the signals recovered by the models differ substantially. Indeed, the baseline solution exhibits spurious oscillations and a large total variation, whereas the inverse-designed model recovers a much more sharply piecewise-constant signal, closely matching the ground truth. The evolution of $\text{TV}(\theta)$ during training confirms that, despite not being optimized explicitly, total variation reduction is consistently pursued by the dynamics induced by the inverse-designed parameter structure.

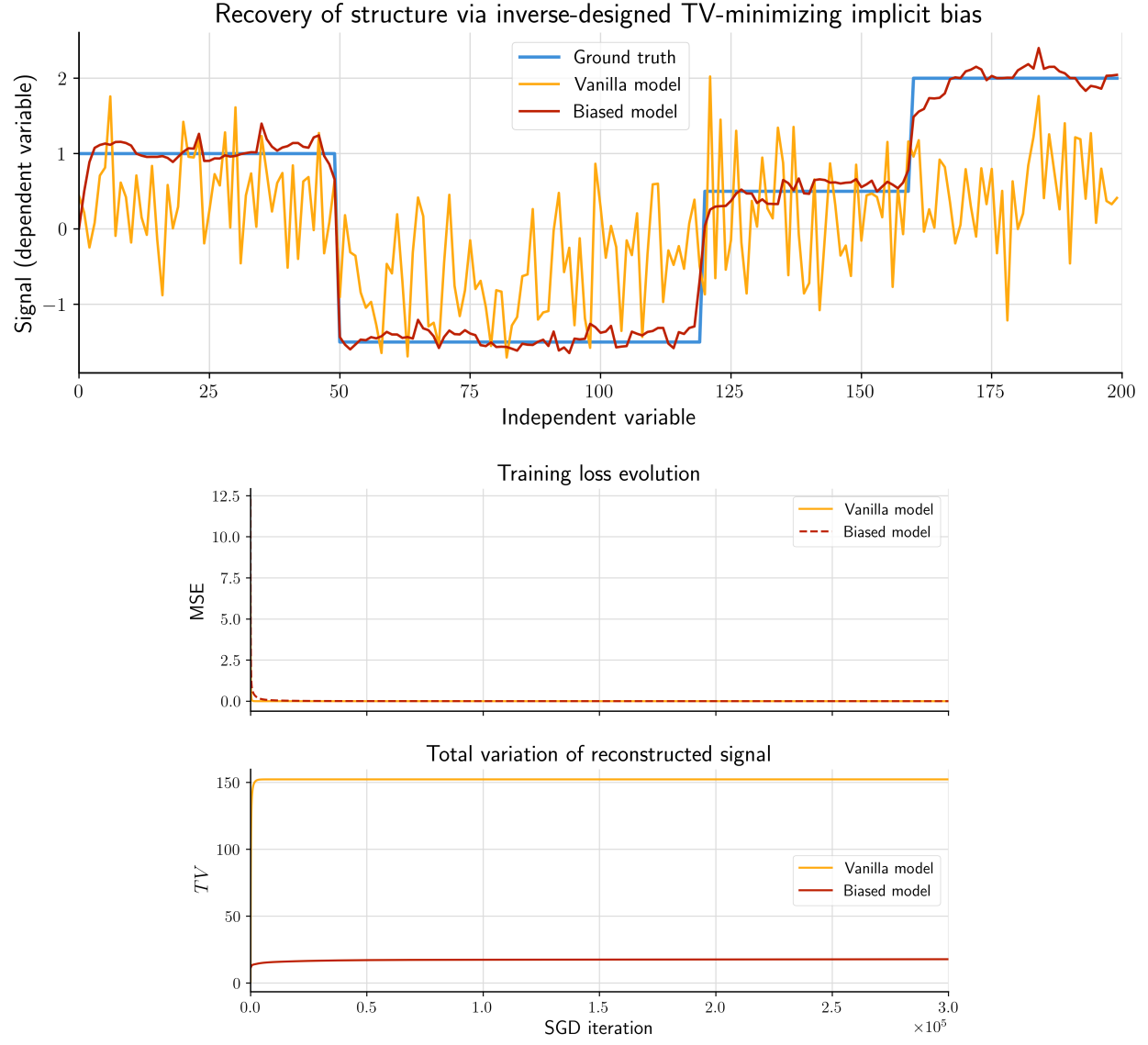


Figure 4: **Top** The *vanilla*, unbiased and not regularized, model fails to capture effectively the underlying piecewise-constant structure of the training signal and the predictor exhibits a significant noisy behaviour. The biased model, obtained via the inverse-designed implicit bias on total variation, and no additional regularization, closely adheres to the target signal and exhibits low local noise. **Middle, Bottom** Both the *vanilla* and biased models rapidly converge to almost-zero loss over the training signal, and – correspondingly – to stable amounts of total variation. The resulting total variation in the *vanilla* model is more than six times that of the *biased* model. Note that the *vanilla* model, on the other hand, still achieves statistical error minimization – though at the cost of complete loss of structure in the recovered signal.

4.2 Matrix factorization IB

Matrix factorization inverse design via channel coupling. To showcase the possibility of engineering a matrix factorization implicit bias, we consider a multi-channel regression problem to be solved by a linear model

$$Y = XW, \quad X \in \mathbb{R}^{N \times D}, W \in \mathbb{R}^{D \times C},$$

where $Y \in \mathbb{R}^{N \times C}$, being C the number of ‘channels’. The design matrix X is sampled at random from a standard normal multivariate distribution with diagonal covariance, and corresponding ground-truth outputs are obtained linearly as $Y_{\text{true}} = XW_{\text{true}}$. The W_{true} matrix is generated as $W_{\text{true}} = P_{\text{true}}Q_{\text{true}}$, with $P_{\text{true}} \in \mathbb{R}^{D \times r}$, $Q_{\text{true}} \in \mathbb{R}^{r \times C}$, and $r \ll \min(D, C)$, thus inducing in $W_{\text{true}}^\top W_{\text{true}}$ a strongly anisotropic spectrum with a pronounced spectral gap (in the experiments, of at least two orders of magnitude) between the first two eigenvalues.

Training data are produced by generating outputs Y_{true} , and further corrupting them with isotropic Gaussian noise (variance: 0.04). Models are optimized by SGD to recover the dense matrix W , under the drive of output reconstruction MSE. Generalization is evaluated on a large independent test set of randomly-sampled inputs and non-corrupted outputs.

Given the randomness of the design matrix, such that no sparsity or local structure deliberately exist in the input representation, any learning effort must solely rely from the presence of structure in the output channels.

We compare three models trained without any explicit regularization:

1. a *naive* model that directly parameterises W ;
2. a *scalar* factorization model $W = P \odot Q$, where the Hadamard product enforces coordinate-wise decoupling across channels, and thus element-wise sparsity in the resulting matrix;
3. a *matrix* factorization model $W = PQ$, which introduces the continuous symmetry

$$(P, Q) \mapsto (PR, R^{-1}Q), \quad R \in \text{GL}(r),$$

and therefore couples all output channels through a shared latent subspace that favors a sparse spectral solution. This corresponds to the simplest case introduced in subsection 4.2 where $\mathcal{A} = I$.

Unlike in the scalar factorization case, where symmetry manifests independently on each coordinate, in the matrix factorization symmetry mixes channels and induces a genuinely collective geometrical structure. The corresponding implicit bias is therefore not steering the model towards coordinate-wise sparsity, but towards a collectively *low-rank structure*. The induced stochastic dynamics favours solutions where the spectrum concentrates in a small number of shared directions across all outputs.

As shown in Figure 5, only the matrix parameterization reliably recovers the correct low-rank structure of the ground truth model, and yields superior test performance, demonstrating an implicit bias toward solutions with a shared low-dimensional channel structure rather than element-wise sparsity.

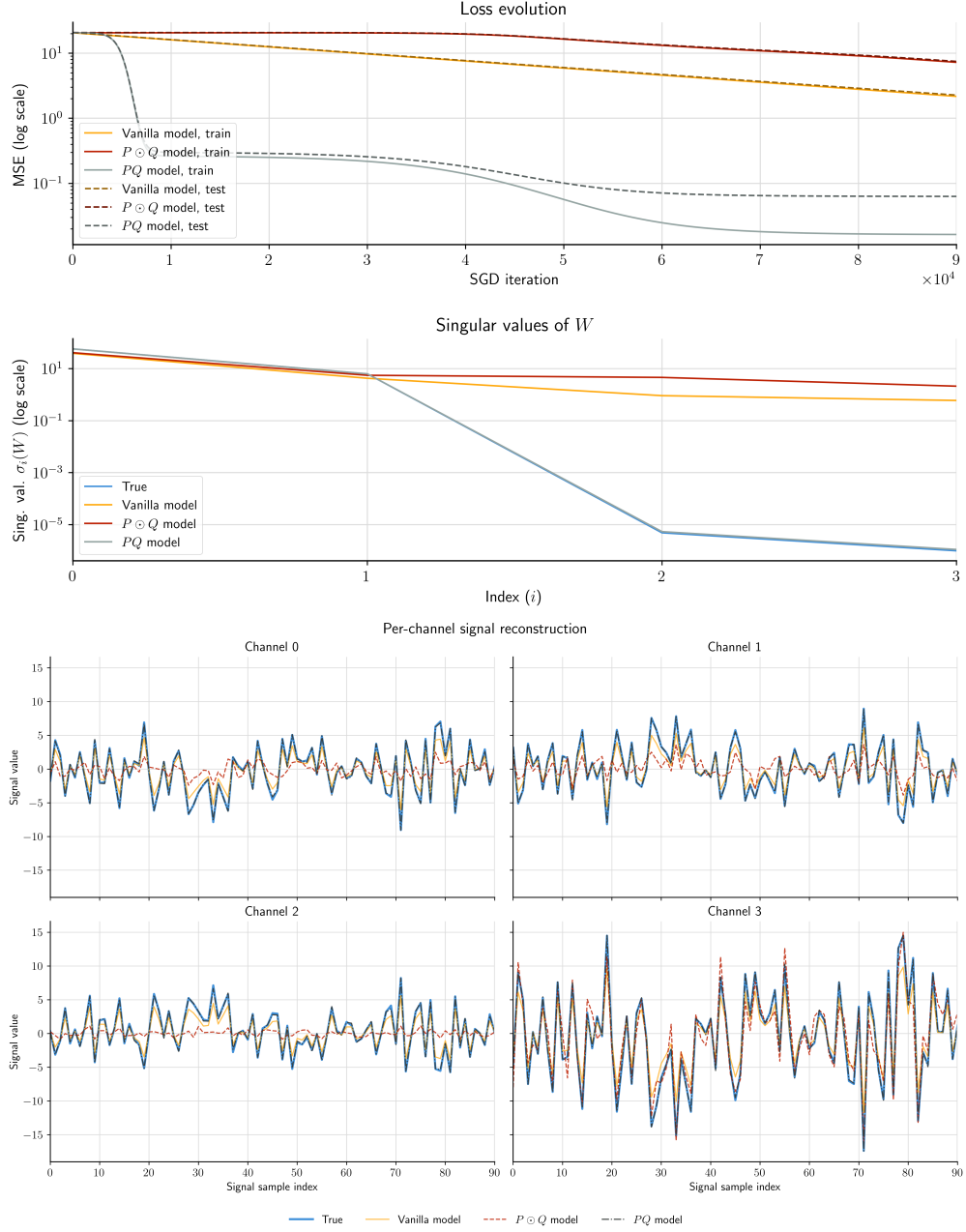


Figure 5: **Top** Train/test learning curves for the three parameterizations. Although all models can drive the training MSE down, the naive and scalar factorization model exhibits markedly worse generalization. The matrix factorization instead achieves a substantially lower test error and stabilizes earlier, indicating that the induced geometric bias is aligned with the ground-truth structure. **Middle** Singular values of the learned weight matrix W . The ground truth is strongly low-rank, with a pronounced spectral gap (i is the channel index). The naive model spreads energy across many singular directions (consistent with an approximately isotropic, Frobenius-type bias), and the scalar factorization has a similar behavior. In contrast, the matrix factorization model closely matches the true singular spectrum, recovering the correct effective rank. **Bottom** Channel reconstructions on a dense evaluation grid. The matrix factorization model tracks the ground truth across channels uniformly, reflecting recovery of the shared low-dimensional channel subspace. The naive and scalar factorization model reconstructions are poorer.

5 Symmetry induces implicit bias of some known Architectures

We now briefly show that many architectures commonly used in machine learning naturally fall into the symmetry classes analyzed in the previous sections. Rather than re-deriving their implicit biases, we identify the specific parameter symmetries induced by each parameterization and explain how these symmetries place the architecture within either the scalar or matrix inverse-design factorization framework. Once the symmetry type is defined, the form of the symmetry-induced implicit bias follows directly from the propositions Proposition 2 and Proposition 3. For mathematical details on the derivations and related numerical experiments we refer to Appendix A. Some examples are also reported in section 6 (i.e. low rank matrix factorization and attention).

We emphasize that a subset of the results reported below has previously appeared in the literature, derived using a variety of different approaches. The purpose of our exposition is that of showing that these results can be recovered in a unified and systematic manner within the new mathematical framework proposed.

Low-rank matrix factorization and attention mechanism. For $W = UV^\top$ or $\mathcal{A}(Q, K) = QK^\top$ This parameterization induces a spectral implicit bias, corresponding to independent logarithmic penalties on the singular values of W or Q, K matrices, favouring a low-rank structure and equivalence of the columns' norms of the factor matrices.

Deep fully-connected or convolutional ReLU neural network.

Across layers we have the factorization across in and out channel of the layers resulting implicit bias enforces channel-wise norm balancing.

Canonical Polyadic (CP) tensor decomposition. A multi-linear model parameterized via a CP decomposition takes the form

$$f(x^{(1)}, x^{(2)}, x^{(3)}) = \sum_{r=1}^R \langle a_r, x^{(1)} \rangle \langle b_r, x^{(2)} \rangle \langle c_r, x^{(3)} \rangle,$$

or equivalently a tensor

$$T = \sum_{r=1}^R a_r \otimes b_r \otimes c_r.$$

Each rank-one component is invariant under the rescaling symmetry $a_r \mapsto \alpha_r a_r$, $b_r \mapsto \beta_r b_r$, $c_r \mapsto \gamma_r c_r$ with $\alpha_r \beta_r \gamma_r = 1$. Symmetry reduction induces equal norm sharing across tensor modes within each rank-one term, yielding an ℓ_1 -type implicit bias on the CP components and favoring low effective tensor rank.

Tensor Train (TT / Matrix Product State) decomposition. A TT-parameterized multi-linear map can be written as

$$f(x_1, \dots, x_L) = \sum_{\{\alpha_\ell\}} G_1(x_1)_{\alpha_0 \alpha_1} G_2(x_2)_{\alpha_1 \alpha_2} \cdots G_L(x_L)_{\alpha_{L-1} \alpha_L},$$

where the G_ℓ are core tensors with internal bond dimensions r_ℓ . Adjacent cores admit the gauge symmetry

$$G_\ell \mapsto G_\ell A, \quad G_{\ell+1} \mapsto A^{-1} G_{\ell+1}, \quad A \in \mathrm{GL}(r_\ell),$$

which leaves the represented tensor invariant. The induced implicit bias enforces covariance matching between adjacent cores, promoting a balanced representations and favoring parsimonious use of internal bond dimensions.

6 Numerical examples for some known architectures

In the following section, we numerically validate some novel implicit bias predictions outlined in section 5. Additional examples and derivations will be discussed in Appendix A.

Rank-2 matrix completion: independent balancing of singular modes. We consider here the problem of matrix completion, where a model is optimized to recover the entire set of entries of a target matrix, from observations related only to a subset of them. Specifically, we choose the target matrix to be

$$M^* = Q \operatorname{diag}(\sigma_1^*, \sigma_2^*) P^\top, \quad \sigma_1^* > \sigma_2^*,$$

thus having rank 2, and train a factorized model $M(U, V) = UV^\top$ by SGD, on the MSE computed on a randomly-chosen $2/5^{\text{ths}}$ subset of entries.

Following the theory (from proposition 3 but see Appendix A for full worked-out details) we predict a gauge potential

$$L_{\text{gauge}}^{\min} \propto \log \sigma_1^* + \log \sigma_2^*,$$

with $\lambda_{U,i} = \lambda_{V,i} = \sqrt{\sigma_i^*}$, independently for $i = 1, 2$. Figure 6 shows the empirical gauge correction computed along training, decomposed per singular mode. As the loss decreases, SGD continues to drift along the symmetry orbit until both modes independently attain the predicted minima $\log(2\sigma_i^*)$.

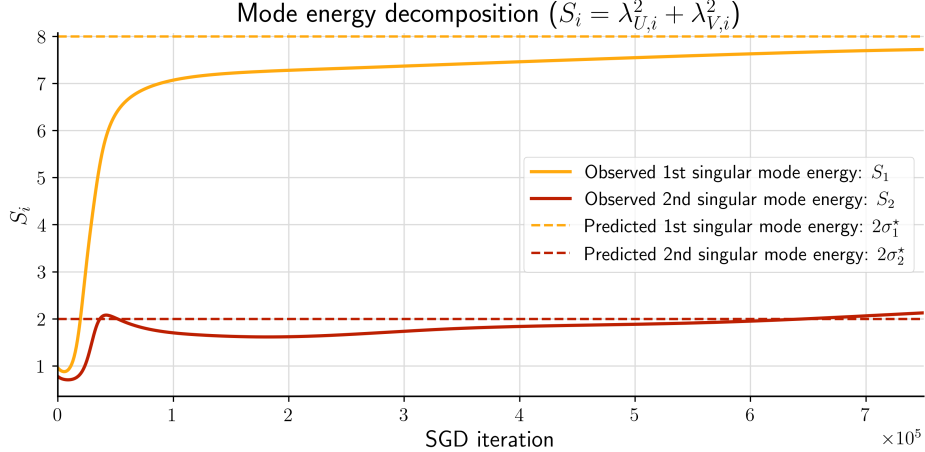


Figure 6: Rank-2 matrix completion experiment. As training progresses under the drive of SGD, parameters explore the $\operatorname{GL}(2)$ group symmetry orbit – finally balancing the two singular modes. The loss reaches a value of 2.55×10^{-5} after 10^6 SGD iterations. **Top** The contribution of each singular mode approaches its theoretically-predicted energy contribution $\log(2\sigma_i^*)$. Such observation confirm the decomposition of gauge potential effects across singular directions. The ordering of modes is arbitrary.

This behaviour is incompatible with minimization of any function of the predictor matrix alone (e.g. Frobenius or nuclear norm). Instead, it highlights the presence of an implicit bias arising from the symmetry-induced geometry of the factorized parameterization. *SGD favours convergence towards those zero-loss solutions that minimize the volume of symmetry orbits under isotropic noise.*

Self-Attention. To validate theoretical derivations for the implicit bias of the scaled dot-product attention mechanism, without letting the specific task at hand influence the results of our analysis – and yet ensuring proper learnability – we make use of the *teacher-student* setup [48]. In such setting, a given neural network architecture with fixed randomly-initialised weights (*teacher*), whose inputs are sampled from a chosen probability distribution, is used to produce ground-truth outputs. A model with identical structure but different parameter initialization (*student*) is then optimised to learn the correct input/output mapping from a given training set. A similarly harvested and labelled validation set is finally used to assess generalization.

In our case, we consider the architecture of multi-head scaled dot-product self-attention [49] in the case of 1 single head (whose details are provided in Appendix A), with all weights initialized by Kaiming initialization [50] (in the teacher, at half the prescribed variance). Inputs are harvested from a standard normal multivariate distribution with diagonal covariance, and the student optimized by SGD on the MSE of the outputs.

In general, self-attention layers admit a parameterization symmetry acting on the query-key space. Indeed, in a single-head attention block, the attention weights depend on the parameters only through the matrix product QK^\top . As a results, the parameterization is invariant under the transformation

$$(Q, K) \longrightarrow (QA, KA^{-\top}), \quad A \in \mathrm{GL}(d),$$

which leaves QK^\top unchanged.

By adequately restricting attention to the diagonal subalgebra, and following the theory, we predict a gauge (proposition 3)

$$L_{\mathrm{gauge}}^{\mathrm{red}} \propto \sum_{i=1}^d \log(\|q_i\|_2^2 + \|k_i\|_2^2).$$

with minima at $\|q_i\|_2 = \|k_i\|_2$ for all indices i .

Figure 7 reports column-wise norms and norms ratios across the query and key matrices. As the loss decreases under the drive of optimization the $\|\|w_{Q,j}\| - \|w_{K,j}\|\|$ mismatch decays until stabilization occurs, demonstrating the predicted *column-wise balancing* induced by the symmetry.

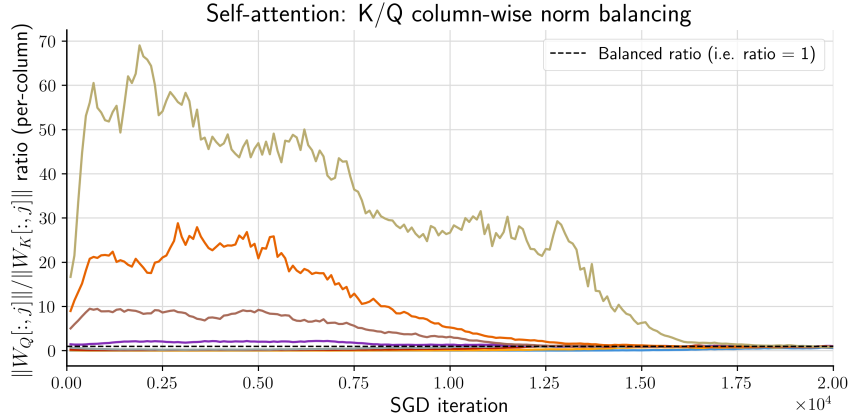


Figure 7: Scaled dot-product self-attention models in a *teacher/student* setup. Training of the student under the drive of SGD converges to balanced key/query columns while reaching a loss $\leq 1.687 \times 10^{-7}$ in 2×10^4 SGD iterations.

7 Discussion and Conclusions

A central idea in statistical mechanics is that macroscopic behavior emerges from microscopic dynamics once redundant degrees of freedom are properly accounted for. In Landau’s theory of phase transitions, symmetry constrains the admissible macroscopic descriptions, while microscopic details affect only non-universal parameters [51]. The very same ideas were later formalized in the theory of renormalization group, where the elimination of microscopic degrees of freedom proceeds through a systematic reduction onto effective variables. Indeed any coarse-graining map induces a symmetry structure by identifying microscopic configurations that correspond to the same macroscopic variable and the resulting effective description is naturally defined on the quotient space, with symmetries given by the transformations that preserve the coarse-graining. [52, 53, 54].

A closely related approach appeared in gauge theory, where the Faddeev–Popov construction was introduced to correctly handle continuous symmetry redundancies in functional integrals [47]. There, equivalent configurations lying on the same symmetry orbit are accounted for by introducing a Jacobian associated with a gauge fixing.

Our framework establishes an analogue formalism in stochastic dynamics – in general – and stochastic *learning* dynamics – in particular – where redundant parameterizations introduce continuous symmetry groups acting on parameter space and stochastic gradient dynamics provides a source of noise. The resulting symmetry-volume (gauge) correction leads to an effective potential, determining specific statistically-favored macroscopic predictors: learning dynamics converges to representatives that concentrate probability mass near minimal-volume orbits. This is the main theoretical contribution of our work: a novel mathematical framework to understand the phenomenon of implicit bias in machine learning and, more in general, in stochastic differential equations (Theorem 1). These result can be seen as a complementary mathematical characterizations ,w.r.t. the one given in the works [44, 29, 32, 30], of the model symmetry related implicit bias.

The other main contribution of this work is the demonstration that a wide class of implicit biases can be *constructively* inverse-designed through the deliberate engineering of parameter symmetries in model structure (proposition 2 and 3). We focused on linear parameter mappings; exploring non-linear generalizations is an important direction for future research.

We believe that the inverse design of models tailored to induce specific implicit biases will be particularly effective for tackling inverse problems that are intrinsically ill-posed across many areas of science. Classical approaches typically rely on explicit regularization or carefully chosen priors to select meaningful solutions. Our results show that analogous effects can instead emerge naturally through model engineering, whereby the structure of the model encodes the desired inductive bias.

Another research direction concerns phase transitions. In learning systems, this concept has been invoked to explain e.g. the phenomenon of grokking, wherein models undergo abrupt transitions from memorization to, e.g. [55]. These transitions can be interpreted as symmetry-driven phase changes in the underlying optimization dynamics. Within our framework, this corresponds to the emergence of a low-volume, symmetry-constrained representation in parameter space.

All our simulations and theory have been developed relying on simple models trained on pseudo-randomly generated synthetic data. This is the regime where we can perfectly fit the data, and we showed that there theory holds. Clearly, in more realistic scenarios, this is not guaranteed to happen and the dynamics, especially in the initial stages of the learning, is not only driven by the geometric gauge term. Nonetheless, the latter is still acting upon learning process across training regimes, with a strength depending on many factors – and whose quantitative study is deferred to

future research.

More broadly, our work reinforces a deep conceptual parallel between theoretical physics (in particular statistical mechanics) and machine learning. In both domains, redundancy in microscopic states leads to macroscopic laws where stochasticity drives the emergence of observable structure due to geometric effects. By unifying symmetry, stochastic dynamics, and implicit bias, we provide a principled framework for understanding and designing inductive biases in learning and physical systems.

References

- [1] Daniel Soudry, Elad Hoffer, Mor Shpigel Nacson, Suriya Gunasekar, and Nathan Srebro. The implicit bias of gradient descent on separable data. *Journal of Machine Learning Research*, 19(70):1–57, 2018.
- [2] Ziwei Ji and Matus Telgarsky. The implicit bias of gradient descent on nonseparable data. In *Proceedings of the 32nd Conference on Learning Theory*, volume 99 of *Pmlr*, pages 1772–1798, 2019.
- [3] Ziwei Ji, Miroslav Dudík, Robert E. Schapire, and Matus Telgarsky. Risk and parameter convergence of logistic regression. *Journal of Machine Learning Research*, 21(73):1–61, 2020.
- [4] Jingfeng Wu et al. Implicit bias of gradient descent for logistic regression at the edge of stability. *arXiv preprint arXiv:2305.11788*, 2023.
- [5] Kaifeng Lyu and Jian Li. Gradient descent maximizes the margin of homogeneous neural networks. In *International Conference on Learning Representations*, 2020.
- [6] Hrithik Ravi, Clayton Scott, Daniel Soudry, and Yutong Wang. The implicit bias of gradient descent on separable multiclass data. In *Advances in Neural Information Processing Systems*, 2024.
- [7] Suriya Gunasekar, Jason D. Lee, Daniel Soudry, and Nathan Srebro. Characterizing implicit bias in terms of optimization geometry. In *Proceedings of the 35th International Conference on Machine Learning*, volume 80 of *Pmlr*, pages 1832–1841, 2018.
- [8] Sanjeev Arora, Nadav Cohen, Wei Hu, and Yuping Luo. Implicit regularization in deep matrix factorization. In *Advances in Neural Information Processing Systems*, volume 32, 2019.
- [9] Mengjia Xu, Akshay Rangamani, Qianli Liao, Tomer Galanti, and Tomaso Poggio. Dynamics in deep classifiers trained with the square loss: Normalization, low rank, neural collapse, and generalization bounds. *Research*, 6, 03 2023.
- [10] Gauthier Gidel, Francis Bach, and Simon Lacoste-Julien. Implicit regularization of discrete gradient dynamics in linear neural networks. In *Proceedings of the 33rd International Conference on Neural Information Processing Systems*, Red Hook, NY, USA, 2019. Curran Associates Inc.
- [11] Hung-Hsu Chou, Carsten Gieshoff, Johannes Maly, and Holger Rauhut. Gradient descent for deep matrix factorization: Dynamics and implicit bias towards low rank. *SSRN Electronic Journal*, 01 2022.
- [12] Lenaic Chizat and Francis Bach. Implicit Bias of Gradient Descent for Wide Two-layer Neural Networks Trained with the Logistic Loss. In *Proceedings of Thirty Third Conference on Learning*

Theory, number 125 in Proceedings of Thirty Third Conference on Learning Theory, pages 1305–1338, Graz / Virtual, Austria, July 2020.

- [13] Andrew R. Barron. Universal approximation bounds for superpositions of a sigmoidal function. *IEEE Transactions on Information Theory*, 39(3):930–945, 1993.
- [14] Behnam Neyshabur, Ryota Tomioka, and Nathan Srebro. In search of the real inductive bias: On the role of implicit regularization in deep learning. In *International Conference on Learning Representations*, 2015.
- [15] Francis Bach. Breaking the curse of dimensionality with convex neural networks. *Journal of Machine Learning Research*, 18(19):1–53, 2017.
- [16] Behnam Neyshabur. *Implicit Regularization in Deep Learning*. PhD thesis, Toyota Technological Institute at Chicago, 2017.
- [17] Gal Vardi. On the implicit bias in deep-learning algorithms. *Commun. ACM*, 66(6):86–93, May 2023.
- [18] Noam Razin and Nadav Cohen. Implicit regularization in deep learning may not be explainable by norms. In *Proceedings of the 34th International Conference on Neural Information Processing Systems*, Nips ’20, Red Hook, NY, USA, 2020. Curran Associates Inc.
- [19] Chang Liu, Wenshuo Huang, and Ryan Y. D. Xu. Implicit bias of deep learning in the large learning rate phase: A data separability perspective. *Applied Sciences*, 13(6):3961, 2023.
- [20] Zhiyuan Li, Tianhao Wang, and Sanjeev Arora. What happens after SGD reaches zero loss? –a mathematical framework. In *International Conference on Learning Representations*, 2022.
- [21] Qianxiao Li, Cheng Tai, et al. Dynamics of stochastic gradient algorithms. *CoRR*, 2015.
- [22] Qianxiao Li, Cheng Tai, et al. Stochastic modified equations and dynamics of stochastic gradient algorithms i: Mathematical foundations. *Journal of Machine Learning Research*, 20(40):1–47, 2019.
- [23] Chiyuan Zhang, Qianli Liao, Alexander Rakhlin, Brando Miranda, Noah Golowich, and Tomaso A. Poggio. Theory of deep learning iib: Optimization properties of SGD. *CoRR*, abs/1801.02254, 2018.
- [24] Stephan Mandt, Matthew D. Hoffman, and David M. Blei. Stochastic gradient descent as approximate bayesian inference. *Journal of Machine Learning Research*, 18(134):1–35, 2017.
- [25] Stephan Mandt, Matthew Hoffman, and David Blei. A variational analysis of stochastic gradient algorithms. In *International conference on machine learning*, pages 354–363. Pmlr, 2016.
- [26] Samuel L. Smith and Quoc V. Le. A bayesian perspective on generalization and stochastic gradient descent. In *International Conference on Learning Representations*, 2018.
- [27] Zeke Xie, Issei Sato, and Masashi Sugiyama. A diffusion theory for deep learning dynamics: Stochastic gradient descent exponentially favors flat minima. In *International Conference on Learning Representations*, 2021.
- [28] Liu Ziyin, Mingze Wang, Hongchao Li, and Lei Wu. Parameter symmetry and noise equilibrium of stochastic gradient descent. *Advances in Neural Information Processing Systems* 37, 2024.

[29] Liu Ziyin. Symmetry induces structure and constraint of learning. In *Proceedings of the 41st International Conference on Machine Learning*, volume 235 of *Proceedings of Machine Learning Research*, pages 62847–62866. Pmlr, 2024.

[30] Liu Ziyin, Yizhou Xu, Tomaso Poggio, and Isaac L. Chuang. Parameter symmetry potentially unifies deep learning theory. *arXiv preprint arXiv:2502.05300*, 2025.

[31] Chih-Yun Chuang and Tomaso Poggio. Topological invariance and the breakdown in learning. *arXiv preprint arXiv:2302.05855*, 2023.

[32] Liu Ziyin, Yizhou Xu, and Isaac L. Chuang. Neural thermodynamics: Entropic forces in deep and universal representation learning. *arXiv preprint arXiv:2505.12387*, 2025. NeurIPS 2025 (poster).

[33] David G. Kendall. A survey of the statistical theory of shape. *Statistical Science*, 4(2):87–99, 1989.

[34] Xavier Pennec. Intrinsic statistics on riemannian manifolds: Basic tools for geometric measurements. *Journal of Mathematical Imaging and Vision*, 25(1):127–154, 2006.

[35] Stephan Huckemann, Thomas Hotz, and Axel Munk. Intrinsic shape analysis: Geodesic principal component analysis for riemannian manifolds modulo lie group actions. *Statistica Sinica*, 20(1):1–100, 2010.

[36] Nina Miolane and Xavier Pennec. Biased estimators on quotient spaces. In *Geometric Science of Information*, volume 9389 of *Lecture Notes in Computer Science*, pages 130–139. Springer, 2015.

[37] Michael Fixman. Classical statistical mechanics of constraints: A theorem and applications to polymers. *The Journal of Chemical Physics*, 69(4):1527–1537, 1974.

[38] Tony Lelièvre, Mathias Rousset, and Gabriel Stoltz. *Free Energy Computations: A Mathematical Perspective*. World Scientific, 2010.

[39] Jean-Paul Ryckaert, Giovanni Ciccotti, and Herman Berendsen. Numerical-integration of cartesian equations of motion of a system with constraints – molecular-dynamics of n-alkanes. *Journal of Computational Physics*, 23:327–341, 03 1977.

[40] Mark Girolami and Ben Calderhead. Riemann manifold langevin and hamiltonian monte carlo methods. *Journal of the Royal Statistical Society: Series B*, 73(2):123–214, 2011.

[41] Yves Grandvalet. Least absolute shrinkage is equivalent to quadratic penalization. In *International Conference on Artificial Neural Networks*, pages 201–206. Springer, 1998.

[42] Peter D Hoff. Lasso, fractional norm and structured sparse estimation using a hadamard product parametrization. *Computational Statistics & Data Analysis*, 115:186–198, 2017.

[43] Clarice Poon and Gabriel Peyré. Smooth bilevel programming for sparse regularization. In *Proceedings of the 35th International Conference on Neural Information Processing Systems*, Nips ’21, Red Hook, NY, USA, 2021. Curran Associates Inc.

[44] Liu Ziyin and Zihao Wang. spred: solving l1 penalty with sgd. In *Proceedings of the 40th International Conference on Machine Learning*, Icml’23. JMLR.org, 2023.

[45] Daniel Kunin, Javier Sagastuy-Brena, Surya Ganguli, Daniel LK Yamins, and Hidenori Tanaka. Neural mechanics: Symmetry and broken conservation laws in deep learning dynamics. *arXiv preprint arXiv:2012.04728*, 2020.

[46] Yongyi Yang and Liu Ziyin. An equivariance toolbox for learning dynamics, 2025.

[47] Ludvig D Faddeev and Victor N Popov. Feynman diagrams for the yang-mills field. *Physics Letters B*, 25(1):29–30, 1967.

[48] David Saad and Sara A. Solla. Exact solution for on-line learning in multilayer neural networks. *Phys. Rev. Lett.*, 74:4337–4340, May 1995.

[49] Ashish Vaswani, Noam Shazeer, Niki Parmar, Jakob Uszkoreit, Llion Jones, Aidan N. Gomez, Łukasz Kaiser, and Illia Polosukhin. Attention is all you need. In *Proceedings of the 31st International Conference on Neural Information Processing Systems*, Nips’17, page 6000–6010, Red Hook, NY, USA, 2017. Curran Associates Inc.

[50] Kaiming He, Xiangyu Zhang, Shaoqing Ren, and Jian Sun. Delving deep into rectifiers: Surpassing human-level performance on imagenet classification. In *Proceedings of the 2015 IEEE International Conference on Computer Vision (ICCV)*, Iccv ’15, page 1026–1034, Usa, 2015. IEEE Computer Society.

[51] L. D. Landau and E. M. Lifshitz. *Statistical Physics, Part I*. Pergamon Press, 3rd edition, 1980.

[52] Nigel Goldenfeld. *Lectures on Phase Transitions and the Renormalization Group*. Taylor and Francis, 1992.

[53] P. M. Chaikin and T. C. Lubensky. *Principles of Condensed Matter Physics*. Cambridge University Press, 1995.

[54] Mehran Kardar. *Statistical Physics of Fields*. Cambridge University Press, 2007.

[55] Bojan Žunkovič and Enej Ilievski. Grokking phase transitions in learning local rules with gradient descent. *Journal of Machine Learning Research*, 25(199):1–52, 2024.

[56] Suriya Gunasekar, Blake Woodworth, Srinadh Bhojanapalli, Behnam Neyshabur, and Nathan Srebro. Implicit regularization in matrix factorization. In *Proceedings of the 31st International Conference on Neural Information Processing Systems*, Nips’17, page 6152–6160, Red Hook, NY, USA, 2017. Curran Associates Inc.

[57] Behnam Neyshabur, Ryota Tomioka, and Nathan Srebro. Norm-based capacity control in neural networks. In *Conference on Learning Theory*, pages 1376–1401, 2015.

[58] Pedro Savarese, Itay Evron, Daniel Soudry, and Nathan Srebro. How do infinite width bounded norm networks look in function space? In *Proceedings of the 32nd Conference on Learning Theory (COLT)*, volume 99 of *Proceedings of Machine Learning Research*, pages 2667–2690, 2019. arXiv:1902.05040.

[59] Suriya Gunasekar, Jason D. Lee, Daniel Soudry, and Nati Srebro. Implicit bias of gradient descent on linear convolutional networks. In *Advances in Neural Information Processing Systems 31 (NeurIPS 2018)*, 2018.

[60] Robert Tibshirani. Regression shrinkage and selection via the lasso. *Journal of the Royal Statistical Society: Series B*, 58(1):267–288, 1996.

- [61] Ming Yuan and Yi Lin. Model selection and estimation in regression with grouped variables. *Journal of the Royal Statistical Society: Series B*, 68(1):49–67, 2006.
- [62] Francis Bach, Rodolphe Jenatton, Julien Mairal, and Guillaume Obozinski. Structured sparsity through convex optimization. *Statistical Science*, 27(4):450–468, 2012.
- [63] Laurent Jacob, Guillaume Obozinski, and Jean-Philippe Vert. Group lasso with overlap and graph lasso. In *Proceedings of the 26th International Conference on Machine Learning (ICML)*, pages 433–440, 2009.

A Symmetry-Induced Implicit Bias in some Known Architectures

Here we provide explicit calculations for the implicit biases of a set of known machine learning techniques and architectures, testing numerically some of them. In doing so, we reproduce some of the results already known from literature [28, 29, 30] from within our novel mathematical framework. All provided examples follow the same general procedure: we first identify the symmetry group model parameterization belongs to, then we analytically compute the orbit Gram matrix associated to such symmetry, we choose a suitable gauge slice, and finally calculate of the minimizer of the resulting gauge loss along symmetry orbits. Once such procedure has been established, we will skip tedious repeated derivations and only record the symmetry group, the resulting constraint Gram matrix, and the minimized gauge condition.

All derivations in this Appendix are performed in the *balanced gauge*, characterized by the condition

$$M(\theta) = H(\theta),$$

with H the Gram matrix induced by the symmetry generators and M is the Faddeev–Popov matrix, the Gram matrix associated with the gauge constraint.

In addition, whenever the symmetry group is non-compact, we restrict attention to a commuting (Abelian) subalgebra of the full Lie algebra (see Paragraph 3.2).

Overview of examples This part of the Appendix is organized as two families of examples, ordered by increasing novelty.

(1) Known implicit biases. We first apply the framework to settings where our implicit bias is already well established, verifying that the gauge picture recovers known results. These include low-rank matrix factorization, where the gauge correction selects balanced factorizations consistent with a nuclear-norm-minimizing bias, and two-layer ReLU networks, where neuron-wise scaling symmetries enforce balanced incoming/outgoing weights across neurons – ultimately matching path- and variation-norm characterizations.

We then consider architectures with well-known symmetries but less understood implicit biases. For convolutional and deeper ReLU networks, we identify frequency- and channel-wise balancing laws induced by translation and scaling symmetries. For self-attention layers, gauge-like transformations of (Q, K, V) yield explicit balancing relations between query, key, and value norms.

All these cases reproduce known results in literature.

(2) New biases for known parameterizations and inverse-designed implicit biases. We consider here tensor-product and tensor-network factorizations, whose symmetry-induced gauge corrections generalize balancing relations to higher-order tensors by means of mode norm equalization. Finally, by following the same logic introduced in section 3, we tackle the inverse problem and design model parameterizations whose symmetries induce desired implicit biases. Examples of such approaches addressed in this appendix include coordinate-wise and block-wise factorizations, which respectively yield *single parameter* and *group ℓ_1* -type sparsity.

A.1 Low-rank matrix factorization

Low-rank matrix factorization is one of the canonical settings where implicit bias has been studied in depth: stochastic gradient descent acting on the factorized model parameterization $M = UV^\top$ is

known to favour low-rank solutions and – under suitable conditions – can be related to nuclear-norm minimization [56] and the symmetry-based results derived in [28]. Here, we show how the same qualitative bias emerges directly from the gauge geometry associated with $\mathrm{GL}(r)$ symmetry of the factorization.

Model and symmetry Let $W^* \in \mathbb{R}^{n \times m}$ be a rank- r matrix ($r \ll \min\{n, m\}$). As described in section 6, we observe a subset of its entries $\Omega \subset \{1, \dots, n\} \times \{1, \dots, m\}$ and fit a factorized model $W(U, V) = UV^\top$, where $U \in \mathbb{R}^{n \times r}$, $V \in \mathbb{R}^{m \times r}$.

For any invertible matrix $R \in \mathrm{GL}(r)$, the transformation

$$(U, V) \mapsto (UR, V(R^{-1})^\top) \quad (24)$$

leaves the product UV^\top invariant.

The correction induced by the gauge has the mode-wise form

$$L_{\text{gauge}}(U, V) = \frac{\sigma^2}{2\beta} \sum_{i=1}^r \log(\lambda_{U,i}^2 + \lambda_{V,i}^2), \quad (25)$$

subject to $\lambda_{U,i} \lambda_{V,i} = \sigma_i^*$.

Therefore, for every singular mode i ,

$$\lambda_{U,i} = \lambda_{V,i} = \sqrt{\sigma_i^*}.$$

Hence, the symmetry-induced gauge geometry selects the *balanced factorization*, in which each singular value of the target matrix is equally decomposed between the two factors.

Numerical validation: gauge bias in rank-2 matrix completion The already introduced problem of matrix completion, studied in section 6 of the main text with a rank-2 matrix, will serve as an example to assess the validity of our theoretical predictions.

Figure 6 reports the empirical evolution of *energies* associated to the symmetry-induced gauge potential of each singular value, comparing it to the value at convergence predicted by our theory. As the training loss decreases, learnable parameters explore under the drive of SGD stochastic noise the symmetry orbit, finally stabilizing in the region where probability volume is minimal.

The result is fully consistent with the theory: SGD does not minimize a simple norm of the weights; instead, its late-stage dynamics selects the balanced factorization that *minimizes local orbit volume under the gauge*.

A.2 Two-layer fully-connected ReLU network

We now turn to one of the classical setting in which the emergence of implicit bias has been described: two-layer fully-connected ReLU networks.

The implicit bias of such models has been extensively studied from the function-space viewpoint—via variation norms, Barron norms, and convex neural network theory [57, 15, 58]. Here, we show that the gauge correction associated with the neuron-wise positive-homogeneity symmetry produces a simple implicit bias: *each neuron is driven to balance the norm of its incoming weights with the magnitude of its outgoing weight*.

We emphasize that the same underlying mechanism as that explored in subsection A.1 is responsible

for such bias: a continuous symmetry in model parameters induces a non-trivial orbit volume element, and in the metric-dual (balanced) gauge this yields an explicit gauge potential that steers optimization towards a specific representative on each orbit.

Model and symmetry Consider the two-layer ReLU network

$$f_\theta(x) = v^\top \text{ReLU}(Wx), \quad W \in \mathbb{R}^{p \times d}, \quad v \in \mathbb{R}^p, \quad \text{ReLU}(z) = \max\{0, z\}.$$

and write the j -th row of W as $w_j^\top \in \mathbb{R}^{1 \times d}$ (or, equivalently, as $w_j \in \mathbb{R}^d$).

Each j^{th} hidden neuron admits a positive-homogeneity symmetry:

$$(w_j, v_j) \mapsto (\alpha_j w_j, \alpha_j^{-1} v_j) \quad (26)$$

for any $\alpha_j > 0$, since $\text{ReLU}(\alpha z) = \alpha \text{ReLU}(z)$ for $\alpha > 0$. The symmetry group is $\mathcal{G} = (\mathbb{R}_{>0})^p$, which – acting independently on each neuron – leads to the following correction

$$L_{\text{gauge}}(W, v) = \frac{\sigma^2}{2\beta} \sum_{j=1}^p \log\left(\|w_j\|_2^2 + v_j^2\right). \quad (27)$$

Minimization along each (neuron-bound) orbit reduces to $\min_{\alpha > 0} (\alpha^2 \|w_j\|_2^2 + \alpha^{-2} v_j^2)$, whose unique minimizer satisfies $\|w_j\|_2^2 = v_j^2$, i.e.,

$$\|w_j\|_2^2 = v_j^2 \quad \iff \quad \|w_j\|_2 = |v_j|. \quad (28)$$

Numerical validation: SGD favours balanced neuron weights in two-layer ReLU networks We empirically validate such theoretical predictions for a ReLU network $f_\theta(x) = v^\top \text{ReLU}(Wx)$ trained by SGD on a linearly-separable binary classification task in \mathbb{R}^2 . In particular, we generate a balanced training set by sampling input data from two distinct standard normal multivariate distributions with diagonal covariance, over the real plane. The output class of each datapoint is determined by the mean of the respective originating distribution: either $(2, 2)$ or $(-2, -2)$. The network is trained by batch-averaged binary cross-entropy (BCE) loss.

The model admits the neuron-wise positive-homogeneity symmetry $(w_j, v_j) \mapsto (\alpha_j w_j, \alpha_j^{-1} v_j)$, under which the represented function of the inputs is invariant.

To quantify convergence toward the gauge-favoured representative on each symmetry orbit, we monitor the per-neuron *balance ratio*

$$\rho_j(t) := \frac{\|w_j(t)\|_2}{|v_j(t)|},$$

for neurons with $v_j(t) \neq 0$. The minimizer of the gauge potential corresponds to predictors where $\rho_j(t) = 1$, i.e. $\|w_j(t)\|_2 = |v_j(t)|$.

Figure 8 collects balance ratios during training, across all network neurons whose pre-activation belongs to the positive semiaxis (and thus is not suppressed by the activation). As training minimises the BCE loss, stochastic noise from SGD drives the exploration along the (approximate) symmetry orbits and biases the dynamical evolution of each *active* neuron toward $\rho_j(t) \rightarrow 1$. This behaviour cannot be explained by the path/variation norm $\sum_j |v_j| \|w_j\|_2$, which is invariant under the same parameterization, but is consistent with the gauge correction we derive. Among equivalent parameterizations of the same predictor, SGD steers learning towards the *balanced* representative of each symmetry-induced orbit.

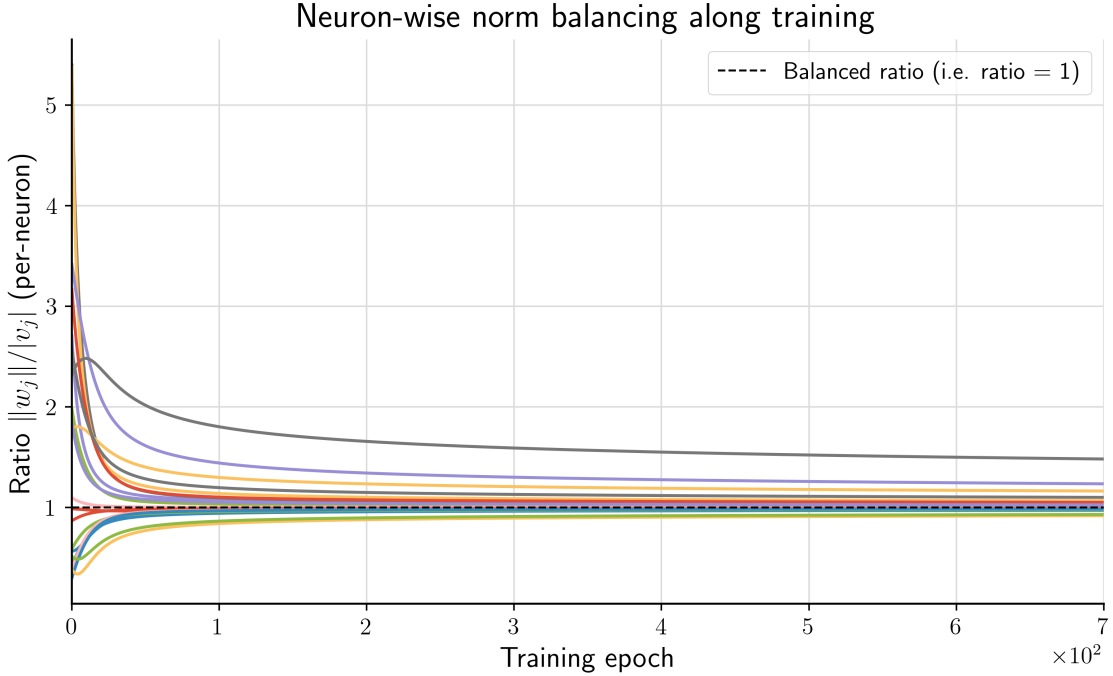


Figure 8: Two-layer ReLU network experiment. The per-neuron balance ratios $\rho_j(t) = \|w_j(t)\|_2/|v_j(t)|$ approach 1 during training under SGD, indicating convergence toward the balanced neuron condition $\|w_j\|_2 = |v_j|$. In this run, the training loss decreases to 1.2×10^{-2} after 7×10^2 epochs. This supports the prediction that SGD exhibits an implicit preference for the gauge-selected representative on each symmetry orbit.

A.3 Two-Layer Linear Circulant Convolutional Networks

We now analyze the linear two-layer convolutional model:

$$f_{w,v}(x) = v^\top (w * x), \quad w, v, x \in \mathbb{R}^L,$$

where $*$ denotes circular convolution on length- L signals.

Let F be the unitary discrete Fourier transform (DFT), and denote $\hat{w} := Fw$, $\hat{v} := Fv$, $\hat{x} := Fx$. Since convolution diagonalizes in the Fourier basis,

$$w * x = F^*(\hat{w} \odot \hat{x}),$$

and by unitarity of F ,

$$f_{w,v}(x) = \langle v, w * x \rangle = \sum_{\omega=0}^{L-1} \overline{\hat{v}(\omega)} \hat{w}(\omega) \hat{x}(\omega). \quad (29)$$

Thus the predictor depends on the frequency-wise products

$$c(\omega) := \overline{\hat{v}(\omega)} \hat{w}(\omega), \quad \omega = 0, \dots, L-1. \quad (30)$$

In the Fourier domain, (30) is invariant under the frequency-wise positive scaling

$$\hat{w}(\omega) \mapsto \alpha(\omega) \hat{w}(\omega), \quad \hat{v}(\omega) \mapsto \alpha(\omega)^{-1} \hat{v}(\omega), \quad \alpha(\omega) > 0, \quad (31)$$

Hence, the correction is

$$L_{\text{gauge}}(\hat{w}, \hat{v}) = \frac{\sigma^2}{2\beta} \sum_{\omega=0}^{L-1} \log(|\hat{w}(\omega)|^2 + |\hat{v}(\omega)|^2), \quad (32)$$

where σ^2 is the usual noise-prefactor.

Using the same argument as in the previous sections when performing the minimization, for every frequency ω ,

$$|\hat{w}(\omega)|^2 = |\hat{v}(\omega)|^2 \iff |\hat{w}(\omega)| = |\hat{v}(\omega)|. \quad (33)$$

Thus the gauge geometry favours predictors exhibiting a *frequency-wise balanced factorization*.

A.4 Deep Linear Circulant Convolutional Networks. Reproducing the result of ([59])

Next, we consider a depth- L linear convolutional network with circulant kernels $w_1, \dots, w_L \in \mathbb{R}^N$ and readout $v \in \mathbb{R}^N$,

$$f_\theta(x) = v^\top C_L(w_L) \cdots C_1(w_1)x, \quad \theta = (v, w_1, \dots, w_L).$$

Let F be DFT, and write $\hat{w}_\ell := Fw_\ell$, $\hat{v} := Fv$, $\hat{x} := Fx$. Since circulant convolution diagonalizes in the Fourier basis, the model decouples across frequencies and we have (Plancharel theorem):

$$f_\theta(x) = \sum_{\omega=0}^{N-1} \overline{\hat{v}(\omega)} \left(\prod_{\ell=1}^L \hat{w}_\ell(\omega) \right) \hat{x}(\omega).$$

For each frequency ω , define the end-to-end Fourier coefficient

$$\hat{\theta}(\omega) := \prod_{\ell=1}^L \hat{w}_\ell(\omega), \quad c(\omega) := \overline{\hat{v}(\omega)} \hat{\theta}(\omega) = \overline{\hat{v}(\omega)} \prod_{\ell=1}^L \hat{w}_\ell(\omega),$$

so the predictor depends on $\{c(\omega)\}_{\omega=0}^{N-1}$. And the correction is

$$L_{\text{gauge}}(\theta) = \frac{\sigma^2}{2\beta} \sum_{\omega=0}^{N-1} \log \left[\left(\prod_{\ell=1}^L |\hat{w}_\ell(\omega)|^2 \right) \left(1 + |\hat{v}(\omega)|^2 \sum_{\ell=1}^L \frac{1}{|\hat{w}_\ell(\omega)|^2} \right) \right]. \quad (34)$$

We fix ω and consider parameters along the scaling orbit, which leaves $c(\omega)$ invariant. At this frequency, the invariant magnitude is

$$|c(\omega)|^2 = |\hat{v}(\omega)|^2 \prod_{\ell=1}^L |\hat{w}_\ell(\omega)|^2.$$

Then, define

$$a_\ell(\omega) := |\hat{w}_\ell(\omega)|^2, \quad b(\omega) := |\hat{v}(\omega)|^2, \quad C(\omega) := |c(\omega)|^2,$$

so that the orbit constraint is expressed as $b(\omega) \prod_{\ell=1}^L a_\ell(\omega) = C(\omega)$. The determinant appearing in the gauge loss is

$$\det H^{(\omega)} = \left(\prod_{\ell=1}^L a_\ell \right) \left(1 + b \sum_{\ell=1}^L \frac{1}{a_\ell} \right) = \left(\prod_{\ell=1}^L a_\ell \right) + C(\omega) \sum_{\ell=1}^L \frac{1}{a_\ell}.$$

This objective is symmetric in (a_1, \dots, a_L) , so any minimizer satisfies $a_1 = \dots = a_L =: t(\omega)$. Substitution gives

$$\det H^{(\omega)} = t(\omega)^L + C(\omega) \frac{L}{t(\omega)},$$

whose unique minimizer solves $t(\omega)^{L+1} = C(\omega)$. Hence,

$$|\hat{w}_1(\omega)|^2 = \dots = |\hat{w}_L(\omega)|^2 = |\hat{v}(\omega)|^2 = |c(\omega)|^{2/(L+1)}.$$

Equivalently,

$$|\hat{w}_1(\omega)| = \dots = |\hat{w}_L(\omega)| = |\hat{v}(\omega)| = |c(\omega)|^{1/(L+1)} \quad \text{for each } \omega. \quad (35)$$

Thus, the gauge geometry favours a predictor whose invariant coefficient $c(\omega)$ is factorized in a *frequency-wise balance* across the L convolutional layers and the readout.

If one absorbs the readout into the last convolutional layer (or equivalently, considers a depth- L factorization of the end-to-end filter $\hat{\theta}(\omega) = \prod_{\ell=1}^L \hat{w}_\ell(\omega)$ without a separate readout), the same balancing argument yields $|\hat{w}_1(\omega)| = \dots = |\hat{w}_L(\omega)| = |\hat{\theta}(\omega)|^{1/L}$ and the associated mode-wise effective bias scales like $|\hat{\theta}(\omega)|^{2/L}$, recovering the implicit $\ell_{2/L}$ Fourier bias reported in [59]. With an additional trainable readout v , the corresponding exponent applies to the invariant $c(\omega) = \overline{\hat{v}(\omega)} \hat{\theta}(\omega)$ and becomes $2/(L+1)$, reflecting that $c(\omega)$ is factorized into $L+1$ multiplicative terms.

A.5 ReLU Convolutional Networks: Breaking of linear symmetry

In the linear convolutional model, frequency-wise phase rotations $\hat{w}(\omega) \mapsto e^{i\alpha(\omega)} \hat{w}(\omega)$ are symmetries because convolution is diagonal in the Fourier domain and no activation function alters such linearity. Such argument breaks in the case of nonlinearly-activated convolutional networks

$$f_{w,v}(x) = v^\top \phi(C(w)x), \quad w, v, x \in \mathbb{R}^L,$$

where the activation ϕ is applied in signal space (i.e. not in the Fourier domain) before the readout. Consequently, the continuous frequency-wise phase symmetry of linear convolution is broken by the non-linearity.

Residual discrete symmetry: cyclic shifts. Although the continuous spectral symmetry is broken, convolutional ReLU networks retain the *finite* group of cyclic shifts:

$$(w, v) \mapsto (T_g w, T_{-g} v), \quad g \in \mathbb{Z}_L. \quad (36)$$

Indeed, circular convolution commutes with shifts and the activation $\phi = \text{ReLU}$ is applied element-wise. This leads to $C(T_g w)x = T_g(C(w)x)$ and $\text{ReLU}(T_g h) = T_g \text{ReLU}(h)$, hence $(T_{-g} v)^\top T_g y = v^\top y$. Because \mathbb{Z}_L is discrete, it generates no continuous orbits and therefore no log-determinant gauge term. Nevertheless, discrete symmetries can still induce a non-trivial bias when SGD noise spreads in probability across finite orbits of equivalent parameters, as discussed at length in Appendix C.

Residual continuous symmetries: channel-wise positive scaling. While nonlinear activations break the rich spectral symmetry of the linear convolutional setting, the positive *homogeneity* of ReLUs, i.e. $\text{ReLU}(\alpha h) = \alpha \text{ReLU}(h)$ preserves a continuous scaling symmetry across channels.

Consider a C -channel convolutional ReLU network:

$$f_{W,v}(x) = \sum_{j=1}^C v_j^\top \text{ReLU}(C(w_j)x), \quad W = (w_1, \dots, w_C), \quad v = (v_1, \dots, v_C), \quad w_j, v_j \in \mathbb{R}^L.$$

Each channel j may be rescaled independently via

$$w_j \mapsto \lambda_j w_j, \quad v_j \mapsto \lambda_j^{-1} v_j, \quad \lambda_j > 0, \quad (37)$$

leaving $f_{W,v}$ unchanged for any input. Thus, the parameterization contains a C -dimensional Lie symmetry group isomorphic to $(\mathbb{R}_{>0})^C$, acting as multiplicative gauge transformations on each channel.

The correction is

$$L_{\text{gauge}}(W, v) = \frac{\sigma^2}{2\beta} \sum_{j=1}^C \log(\|w_j\|_2^2 + \|v_j\|_2^2), \quad (38)$$

whose unique minimizer satisfies

$$\|w_j\|_2^2 = \|v_j\|_2^2 \iff \|w_j\|_2 = \|v_j\|_2, \quad \text{for every channel } j. \quad (39)$$

Of course, if v_j is scalar in a given architecture, this reduces to the $\|w_j\|_2 = |v_j|$ balance we previously derived.

In a multi-layer convolutional network, the same argument applies layer-wise – yielding the *channel-balancing* law

$$\|w_{\ell,j}\|_2 \approx \|v_{\ell,j}\|_2 \quad \text{independently for each channel } (\ell, j).$$

Three critical differences from the linear convolutional case follow immediately:

1. The frequency-wise phase symmetry of linear convolution is broken; the only exact continuous symmetry remaining here is channel-wise scaling, which acts uniformly across all Fourier components of a channel.
2. The gauge correction selects a *representative* within each scaling equivalence class, fixing the relative magnitudes of (w_j, v_j) but not the invariant predictor quantity carried by that channel.
3. Along a scaling orbit, the gauge term has a unique minimum at the balanced point and increases away from it in either direction.

Thus, nonlinear activations flatten most of the linear convolutional symmetry geometry, leaving behind precisely C balancing relations—one per channel—as the dominant continuous symmetry-induced implicit bias mechanism.

Remark 1 (Polynomial and homogeneous non-linearities). The collapse of the rich Fourier-phase symmetry of linear convolutions, in ReLU networks, is not specific to the rectifier activation. What fundamentally survives in the general case is symmetry induced by *positive homogeneity*.

If an activation function ϕ is homogeneous of degree $k > 0$, then $\phi(\alpha h) = \alpha^k \phi(h)$ for all $\alpha > 0$ (e.g. $\phi(h) = h^k$). As a consequence, each convolutional channel of a ϕ -activated convolutional network retains an exact continuous scaling symmetry

$$w_j \mapsto \lambda_j w_j, \quad v_j \mapsto \lambda_j^{-k} v_j, \quad \lambda_j > 0,$$

which leaves the predictor invariant.

Differentiating at $\lambda_j(t) = e^{ta_j}$ yields the symmetry group generator $\delta w_j = a_j w_j$, $\delta v_j = -k a_j v_j$, and thus the orbit Gram matrix entry becomes:

$$\langle \xi_{e_j}, \xi_{e_j} \rangle = \|w_j\|_2^2 + k^2 \|v_j\|_2^2,$$

The corresponding gauge correction is given by

$$L_{\text{gauge}} = \frac{\sigma^2}{2\beta} \sum_j \log(\|w_j\|_2^2 + k^2\|v_j\|_2^2). \quad (40)$$

Minimizing such potential along the scaling orbit yields a generalized balancing relation; under the Euclidean metric used here, the minimizing representative satisfies

$$\|w_j\|_2^2 = k^3\|v_j\|_2^2 \quad \iff \quad \|w_j\|_2 = k^{3/2}\|v_j\|_2.$$

As a sanity check, being ReLU a 1-homogeneous activation function, fixing $k = 1$ in the expression recovers the balancing law previously derived.

Remark 2 (Smooth non-linearities and approximate spectral bias). Although ReLU activations breaks the continuous Fourier-phase symmetry of linear convolutions, smooth activation functions – although non-linear – behave approximately as affine operators over limited regions of the domain, such as those typically explored in the later-stage optimization of neural network models. In this specific setting, the dynamics of a nonlinearly-activated convolutional model is close to that of a linear convolutional model, and the spectral symmetry is only weakly broken. As a result, channel-wise positive-scaling symmetry remains exact, while a frequency-dependent gauge effect may persist approximately, with its strength dependent on the curvature of the activation.

A.6 Deep fully-connected ReLU networks

We now extend the two-layer ReLU analysis to deeper fully-connected networks with positively homogeneous *elementwise* activations.

The crucial aspect of our analysis is that the homogeneity-induced scaling symmetry acts *locally* at the level of each hidden neuron: it allows the rescaling of the incoming weights to that neuron, as long as an inverse rescaling of its outgoing weight(s) ensures the balance. Consequently, the orbit geometry (and hence the gauge correction) decomposes neuron-wise and layer-wise.

Consider a depth- L network

$$f_\theta(x) = W_L \phi(W_{L-1} \phi(\cdots \phi(W_1 x) \cdots)), \quad \theta = (W_1, \dots, W_L),$$

where ϕ is positively homogeneous: $\phi(\alpha z) = \alpha \phi(z)$ for $\alpha > 0$. Let d_ℓ denote the width of layer ℓ (so $W_\ell \in \mathbb{R}^{d_\ell \times d_{\ell-1}}$). For diagonal scaling matrices $D_\ell = \text{diag}(\alpha_{\ell,1}, \dots, \alpha_{\ell,d_\ell})$, the reparameterization

$$W_1 \mapsto D_1 W_1, \quad W_\ell \mapsto D_\ell W_\ell D_{\ell-1}^{-1} \quad (2 \leq \ell \leq L-1), \quad W_L \mapsto W_L D_{L-1}^{-1}, \quad (41)$$

leaves f_θ invariant.

The correction is

$$L_{\text{gauge}}(\theta) = \frac{\sigma^2}{2\beta} \sum_{\ell=1}^{L-1} \sum_{j=1}^{d_\ell} \log\left(\|w_{\ell,j}^{\text{in}}\|_2^2 + \|w_{\ell,j}^{\text{out}}\|_2^2\right). \quad (\text{H3})$$

Restricting to the scaling orbit of a single neuron (ℓ, j) , $(w_{\ell,j}^{\text{in}}, w_{\ell,j}^{\text{out}}) \mapsto (\alpha w_{\ell,j}^{\text{in}}, \alpha^{-1} w_{\ell,j}^{\text{out}})$, and the same argument described in the two-layer case yields a unique minimizer at the balanced point:

$$\|w_{\ell,j}^{\text{in}}\|_2 = \|w_{\ell,j}^{\text{out}}\|_2 \quad \text{for all hidden neurons } (\ell, j). \quad (42)$$

This generalization matches the two-layer ReLU result: the symmetry alone governs how representation norm is distributed locally across incoming and outgoing connections, independent of the specific function collectively expressed by the predictor.

A.7 Deep convolutional ReLU networks: residual implicit bias

Deep convolutional ReLU architectures have two distinct classes of parameter symmetries. First, as in the one-layer convolutional ReLU setting of subsection A.5, the nonlinearity breaks the rich *spectral* (phase) symmetries present in linear convolutions, so that no frequency-wise continuous orbit geometry survives. Second, the network retains (i) a discrete cyclic-shift symmetry and (ii) a continuous positive-scaling symmetry induced by homogeneity.

Discrete symmetry: cyclic shifts. A convolutional layer is equivariant to circular shifts, and in particular the joint reparameterization

$$(w, v) \mapsto (T_g w, T_{-g} v), \quad g \in \mathbb{Z}_L, \quad (43)$$

preserves the represented function (see Equation (36) in subsection A.5). Since \mathbb{Z}_L is discrete, it has no infinitesimal generators and therefore produces no continuous orbit metric and no log-determinant gauge correction (i.e., it produces no $\log \det H$ correction to the dynamics). Its effect is purely combinatorial through orbit size, as described in Appendix C.

Continuous symmetry: channel-wise positive scaling This type of symmetry and induced gauge are the same as those already described in subsection A.6, when describing deep ReLU-activated fully-connected networks.

Consider a deep convolutional ReLU network with linear mixing across channels at each convolutional layer. Clearly, its activations satisfy the relation $\text{ReLU}(\alpha z) = \alpha \text{ReLU}(z)$. Then, each hidden channel (ℓ, j) admits a positive-scaling symmetry that rescales the channel output of layer ℓ and compensates by the inverse rescaling of the incident weights in layer $\ell + 1$. In complete analogy with the deep fully-connected ReLU case (subsection A.6), the continuous symmetry group is a product of independent scaling across channels, i.e.

$$\mathcal{G} \cong \prod_{\ell=1}^{L-1} (\mathbb{R}_{>0})^{C_\ell},$$

and its Lie algebra acts locally on the incoming and outgoing parameter blocks incident to each channel.

The same balanced gauge of subsection A.6 holds in this case, giving $M = H$ and thus $G_\chi = H$ channel-wise. The resulting gauge correction has the same form as (H3), and its minimization on each scaling orbit yields the balancing law

$$\|w_{\ell,j}^{\text{in}}\|_2 = \|w_{\ell,j}^{\text{out}}\|_2, \quad \text{for all hidden channels } (\ell, j), \quad (44)$$

Such law is equivalent to $\|w_{\ell,j}^{\text{out}}\|_2 = \|w_{\ell+1,j}^{\text{in}}\|_2$, under the standard identification of incoming weights of channel j at layer $\ell + 1$ with outgoing weights of channel (ℓ, j) .

Comparison with fully-connected networks. Our analysis of symmetries shows that deep convolutional ReLU networks and deep fully-connected ReLU networks share the *same* surviving *continuous* parameter symmetry mechanism: local positive scaling induced by homogeneity. Accordingly, the gauge-induced geometric correction dependent on such specific symmetry has identical form across both architectures, and leads to the same class of balancing laws.

This does *not* imply – however – that the global implicit bias in *function space* is the same. Convolutions impose strong architectural constraints (weight sharing, locality, translation equivariance) that shape *which functions* are effectively representable and therefore *which predictors* are favored. By contrast, the gauge correction governs *how* probability mass is distributed among *equivalent parameterizations* that realize the same predictor function. In addition, discrete symmetries (cyclic shifts) and spatial structure of intermediate activations can introduce in convolutional architectures further biases absent in fully-connected models.

In summary, the convolutional structure primarily constrains and inductively biases the function class the model is able to express, whereas the gauge mechanism steers learning dynamics towards specific representatives within each symmetry orbit – among those expressing the same predictor. We leave a systematic simulation study of these interacting effects to future work.

A.8 Attention Layers

We turn here our attention to the study of implicit bias induced by symmetries present in attention mechanisms, with particular focus on scaled dot-product self-attention.

Unlike fully-connected or convolutional ReLU network layers, attention mechanisms admit non-trivial $\mathrm{GL}(d)$ reparameterization symmetries, whose effects manifest independently at the level of attention heads. A consequence of this symmetry is a tendency towards neuron/mode-wise balancing between the query and key representation matrices.

Let $x \in \mathbb{R}^{L \times d}$, and consider a single scaled dot-product self-attention head

$$h(x) = A(Q, K) V x, \quad A(Q, K) = \mathrm{softmax}\left(\frac{1}{\sqrt{d}} Q K^\top\right).$$

where $Q, K \in \mathbb{R}^{L \times d}$ (and V is held fixed for the purposes of our discussion on symmetry). The attention weights depend on Q, K only through $Q K^\top$. Thus, the reparameterization

$$(Q, K) \mapsto (Q R, K R^{-T}), \quad R \in \mathrm{GL}(d), \quad (45)$$

preserves $Q K^\top$, and hence the attention map and the loss.

Using the exact same steps as those in the matrix factorization example subsection A.1, we restrict to the diagonal subalgebra, yielding mode-wise decoupling.

Write q_i and k_i for the i -th columns of Q and K , respectively.

The gauge correction is

$$L_{\mathrm{gauge}}(Q, K) = \frac{\sigma^2}{2\beta} \sum_{i=1}^d \log (\|q_i\|_2^2 + \|k_i\|_2^2). \quad (46)$$

Along the diagonal scaling orbit $(q_i, k_i) \mapsto (\alpha_i q_i, \alpha_i^{-1} k_i)$, the rank-one contribution $q_i k_i^\top$ is invariant for each i . As a consequence, in particular, the product $\|q_i\|_2 \|k_i\|_2$ is invariant.

Let $x_i = \|q_i\|_2^2$, $y_i = \|k_i\|_2^2$. Then $x_i \mapsto \alpha_i^2 x_i$, $y_i \mapsto \alpha_i^{-2} y_i$, and $x_i y_i$ is constant along the orbit. Minimizing $x_i + y_i$ such $x_i y_i$ invariance, the gauge term is minimized at the balanced representative:

$$\|q_i\|_2 = \|k_i\|_2 \quad \text{for all } i = 1, \dots, d. \quad (47)$$

Equivalently, on the balanced slice \mathcal{S} one has $\mathrm{diag}(Q^\top Q) = \mathrm{diag}(K^\top K)$. In multi-head attention, the same conclusion applies independently to each head.

Numerical evidence To validate our theoretical predictions, we consider the regression task in a teacher/student setup described in section 6. In detail, both teacher and student models implement the same multi-head (with 1 head only) self-attention layer with token embedding dimension d_{model} and head dimension d_{head} . For an input sequence $x \in \mathbb{R}^{L \times d_{\text{model}}}$, the attention head computes

$$Q = xW_Q, \quad K = xW_K, \quad V = xW_V,$$

$$A = \text{softmax}\left(\frac{QK^\top}{\sqrt{d_{\text{head}}}}\right), \quad h(x) = (AV)W_O \in \mathbb{R}^{d_{\text{model}}},$$

where $(W_Q, W_K, W_V) \in \mathbb{R}^{d_{\text{model}} \times d_{\text{head}}}$ and $W_O \in \mathbb{R}^{d_{\text{head}} \times d_{\text{model}}}$, the output weights, are trainable parameters. The term W_O , in the general multi-head case, will act on the concatenation of head outputs; since here we consider only one head, it acts on its output as a readout matrix. Such technical remark does not impair generalization to the multi-head case.

The *teacher* network is initialized with fixed random weights $(W_Q^*, W_K^*, W_V^*, W_O^*)$ according to Kaiming initialization [50] at half variance, and is queried on i.i.d. Gaussian input token sequences $x \sim \mathcal{N}(0, I)$ to define the target function $y^*(x) = h(x; W^*)$. In such way we ensure no task-specific structure is inadvertently interfering with the bias we want to assess.

The student prediction is given by $y(x; W)$, and training minimizes by SGD (with an addition of further isotropic Gaussian noise proportional to $\sqrt{2\eta/\beta}$, to ensure the diffusive regime throughout all training) on the mean-squared error

$$\mathbb{E}[\|y(x; W) - y^*(x)\|^2].$$

Since the teacher belongs to the same parameterized class as the student, the zero-loss set spans the entire symmetry orbit \mathcal{O}_{W^*} . However, the student weights are also initialized according to Kaiming initialization, but at full variance. Thus, they do belong to the same symmetry orbit as the teacher, but are put in a deliberately *unbalanced gauge* by such variance mismatch.

Already shown Figure 7 confirms our predictions.

A.9 Tensor Factorizations

We examine here the symmetry-induced implicit bias for Canonic Polyadic (CANDECOMP / PARAFAC) tensor factorizations (rank-1 and rank- R), and for Tensor Train (or, equivalently, Matrix Product) factorizations (TT/MPS). Unlike for matrices, no classical convex regularizer is known to characterize SGD in these settings. In our framework, the continuous reparameterization symmetries determine an orbit-volume correction, and its minimizers drive the dynamics towards a balanced representative within each symmetry class.

Rank-1 CP model and symmetry. Let us consider, for example, a tensor-factorized model

$$T = u \otimes v \otimes w \in \mathbb{R}^{d_1 \times d_2 \times d_3}, \quad (48)$$

and make it fit a target $T^* = u^* \otimes v^* \otimes w^*$, by SGD on the MSE loss. The parameterization admits the standard CP scaling symmetry: for any $(a, b, c) \in \mathbb{R}_{>0}^3$ with $abc = 1$,

$$(au) \otimes (bv) \otimes (cw) = u \otimes v \otimes w.$$

Thus, the symmetry group is:

$$\mathcal{G} = \{(a, b, c) \in (\mathbb{R}_{>0})^3 : abc = 1\} \cong (\mathbb{R}_{>0})^2,$$

and each zero-loss solution belongs to a two-dimensional orbit.

Geometry of symmetry directions. Identify the Lie algebra as:

$$\mathfrak{g} = \{(\alpha, \beta, \gamma) \in \mathbb{R}^3 : \alpha + \beta + \gamma = 0\} \cong \mathbb{R}^2,$$

via one-parameter scaling $a(t) = e^{\alpha t}$, $b(t) = e^{\beta t}$, $c(t) = e^{\gamma t}$. Differentiating yields the fundamental vector field

$$\xi_{(\alpha, \beta, \gamma)}(u, v, w) = (\alpha u, \beta v, \gamma w).$$

A convenient (non-orthonormal) basis of \mathfrak{g} is

$$(\alpha, \beta, \gamma) = \alpha(1, 0, -1) + \beta(0, 1, -1),$$

which induces the orbit tangent basis

$$e_1 := \xi_{(1, 0, -1)} = (u, 0, -w), \quad e_2 := \xi_{(0, 1, -1)} = (0, v, -w).$$

Equip parameter space with the Euclidean metric: $\langle(\delta u, \delta v, \delta w), (\delta u', \delta v', \delta w')\rangle = \langle\delta u, \delta u'\rangle + \langle\delta v, \delta v'\rangle + \langle\delta w, \delta w'\rangle$. The orbit Gram matrix $H(u, v, w) \in \mathbb{R}^{2 \times 2}$ in the basis $\{e_1, e_2\}$ is

$$H = \begin{pmatrix} \langle e_1, e_1 \rangle & \langle e_1, e_2 \rangle \\ \langle e_2, e_1 \rangle & \langle e_2, e_2 \rangle \end{pmatrix} = \begin{pmatrix} \|u\|^2 + \|w\|^2 & \|w\|^2 \\ \|w\|^2 & \|v\|^2 + \|w\|^2 \end{pmatrix}, \quad \det H = \|u\|^2\|v\|^2 + \|u\|^2\|w\|^2 + \|v\|^2\|w\|^2.$$

We can choose the (metric-dual) balanced gauge map

$$\chi(u, v, w) := \begin{pmatrix} \frac{1}{2}(\|u\|^2 - \|w\|^2) \\ \frac{1}{2}(\|v\|^2 - \|w\|^2) \end{pmatrix}, \quad \mathcal{S} := \chi^{-1}(0) = \{\|u\| = \|v\| = \|w\|\}.$$

For a variation $(\delta u, \delta v, \delta w)$,

$$d\chi_1 = \langle u, \delta u \rangle - \langle w, \delta w \rangle, \quad d\chi_2 = \langle v, \delta v \rangle - \langle w, \delta w \rangle.$$

Evaluating on the orbit basis vectors e_1, e_2 gives

$$M_{ij} := d\chi_i(e_j) = \begin{pmatrix} \|u\|^2 + \|w\|^2 & \|w\|^2 \\ \|w\|^2 & \|v\|^2 + \|w\|^2 \end{pmatrix} = H.$$

Hence, in this metric-dual gauge, $M = H$ and therefore

$$G_\chi = MH^{-1}M^\top = H.$$

Gauge correction and implicit bias (rank-1). The symmetry-induced gauge term is:

$$L_{\text{gauge}}(u, v, w) = \frac{\sigma^2}{2\beta} \log \det H(u, v, w) = \frac{\sigma^2}{2\beta} \log(\|u\|^2\|v\|^2 + \|u\|^2\|w\|^2 + \|v\|^2\|w\|^2). \quad (49)$$

on the zero-loss manifold. Assuming directions align with the ground truth so that only CP scaling remains, the invariant is the product of norms:

$$\|u\|^2\|v\|^2\|w\|^2 = S := \|u^*\|^2\|v^*\|^2\|w^*\|^2.$$

Let $x = \|u\|^2$, $y = \|v\|^2$, $z = \|w\|^2$. Then, $\det H = xy + xz + yz$ and $xyz = S$. Minimizing $xy + xz + yz$ under $xyz = S$ gives the unique minimizer $x = y = z = S^{1/3}$, hence

$$\|u\| = \|v\| = \|w\|. \quad (50)$$

Order- k CP factorization. We now extend the analysis to rank- R CP factorization of a k -way tensor

$$T = \sum_{r=1}^R u_r^{(1)} \otimes u_r^{(2)} \otimes \cdots \otimes u_r^{(k)}, \quad u_r^{(j)} \in \mathbb{R}^{d_j}.$$

The very same steps done in the case of tensor factorization below, now, lead to the IB:

$$\|u_r^{(1)}\| = \cdots = \|u_r^{(k)}\| = S_r^{1/(2k)}, \quad r = 1, \dots, R. \quad (51)$$

Rank- R Tensor Train (TT) factorization. We now analyze the implicit bias induced by a rank- R Tensor Train (TT) factorization, also known as a Matrix Product State (MPS) in many-body quantum physics. For simplicity, we focus on the case of a three-way tensor $T \in \mathbb{R}^{n_1 \times n_2 \times n_3}$, which admits the TT representation

$$T(i_1, i_2, i_3) = G_1(i_1) G_2(i_2) G_3(i_3),$$

where the cores are matrices of compatible dimensions:

$$G_1(i_1) \in \mathbb{R}^{1 \times r}, \quad G_2(i_2) \in \mathbb{R}^{r \times r}, \quad G_3(i_3) \in \mathbb{R}^{r \times 1}.$$

Writing the contraction over the internal (bond) indices explicitly, yields

$$T(i_1, i_2, i_3) = \sum_{\alpha=1}^r \sum_{\beta=1}^r G_1(1, i_1, \alpha) G_2(\alpha, i_2, \beta) G_3(\beta, i_3, 1). \quad (52)$$

This representation should be compared to the rank- R CP decomposition,

$$T(i_1, i_2, i_3) = \sum_{s=1}^R u_s(i_1) v_s(i_2) w_s(i_3),$$

which expresses the tensor as a *sum* of separable rank-one terms. While CP involves parallel factorization across modes with a scaling symmetry, TT decomposition organizes interactions sequentially through intermediate dimensions. As a result, TT introduces *matrix-valued*, symmetries absent in CP.

Gauge symmetry. TT representations are not unique. For any invertible matrix $A \in \mathrm{GL}(r)$, the transformations

$$G_1 \mapsto G_1 A, \quad G_2 \mapsto A^{-1} G_2 A, \quad G_3 \mapsto A^{-1} G_3,$$

leave the decomposed tensor T invariant. More generally, in a k -core TT, each internal bond carries a $\mathrm{GL}(r_j)$ gauge symmetry. In contrast to CP, where the gauge group acts by scalar rescaling, TT features a gauge group non-trivially acting between adjacent cores.

Orbit geometry and Gram operator. Let $U_1 \in \mathbb{R}^{n_1 \times r}$ and $U_2 \in \mathbb{R}^{(n_2 r) \times r}$ denote the matricizations of G_1 and G_2 , respectively. For an infinitesimal generator $X \in \mathfrak{gl}(r)$, the induced variations along the gauge orbit are

$$\delta U_1 = U_1 X, \quad \delta U_2 = -X U_2.$$

Equipping parameter space with the Euclidean (Frobenius) metric, the resulting orbit Gram bilinear form is:

$$H(X, Y) = \mathrm{tr} \left(X^\top (U_1^\top U_1 + U_2^\top U_2^\top) Y \right).$$

Thus the orbit metric is controlled by the positive-definite matrix

$$G := U_1^\top U_1 + U_2^\top U_2 \in \mathbb{R}^{r \times r}.$$

Gauge correction and bond balancing. The symmetry-induced gauge correction to the stationary distribution takes the form

$$L_{\text{gauge}}(\theta) = \frac{\sigma^2}{2\beta} \log \det(U_1^\top U_1 + U_2^\top U_2),$$

up to additive constants. Minimizing this correction along the gauge orbit determines a canonical representative in which the left and right bond metrics are balanced. A natural gauge-fixing condition is

$$U_1^\top U_1 = U_2^\top U_2,$$

which equalizes the contribution of adjacent cores to the bond geometry. This condition is the Tensor Train analogue of the balancing observed in CP factorizations, but here it arises from a symmetry acting on matrix-valued internal degrees of freedom.

Physics interpretation: tensor networks and entanglement. In quantum notation, TT is exactly the Matrix Product State (MPS) ansatz, where bond dimensions encode entanglement structure. The $\text{GL}(r_j)$ gauge freedom represents basis changes on virtual bond spaces. The symmetry-induced geometry drives the state toward a canonical gauge where bond metrics are balanced, stabilizing the internal representation.

In other words, implicit bias in TT factorization induces an automatic gauge fixing and a stable internal (bond/entanglement) structure.

Table 1 summarizes similarities and differences across implicit biases of the tensor factorizations considered (CP and TT).

Table 1: Gauge symmetries and implicit bias in tensor decompositions.

Model	Symmetry group	Gauge geometry penalizes	Implicit bias outcome
CP	$(\mathbb{R}_{>0})^{R(k-1)}$	imbalance across modes	equal factor norms per component
TT (MPS)	$\prod_{j=1}^{k-1} \text{GL}(r_j)$	bond metric mismatch	balanced (canonical) cores

B PCA

We consider the PCA objective

$$\mathcal{L}(W) = \sum_{x \in \mathcal{B}} \|x - WW^\top x\|^2, \quad W \in \mathbb{R}^{d \times r}.$$

Define the rank- $\leq r$ positive semidefinite matrix

$$P := WW^\top \in \mathbb{R}^{d \times d}, \quad P = P^\top \succeq 0, \quad \text{rank}(P) \leq r.$$

(When $W^\top W = I_r$, P is an orthogonal projector, $P^2 = P$.

Right $O(r)$ symmetry. For any $R \in O(r)$,

$$(WR)(WR)^\top = WRR^\top W^\top = WW^\top,$$

so $\mathcal{L}(W) = \mathcal{L}(WR)$. Thus the learning problem has a compact continuous symmetry group

$$\mathcal{G} = O(r), \quad \mathfrak{g} = \mathfrak{o}(r) = \{A \in \mathbb{R}^{r \times r} : A^\top = -A\}.$$

On the full-rank set $\{W : \text{rank}(W) = r\}$, this right action is free: if $WR = W$, then $W(R - I) = 0$, and since W has full column rank this implies $R = I$.

Orbit metric. An infinitesimal generator $A \in \mathfrak{o}(r)$ acts on W as

$$\delta W = WA.$$

We use the ambient Euclidean inner product $\langle X, Y \rangle = \text{Tr}(X^\top Y)$. Let $\{A_\alpha\}$ be an orthonormal basis of $\mathfrak{o}(r)$ with respect to $\langle A, B \rangle_{\mathfrak{o}(r)} := -\text{Tr}(AB)$. The Gram matrix of the $O(r)$ -orbit at W is

$$\begin{aligned} G_{\alpha\beta}(W) &= \langle WA_\alpha, WA_\beta \rangle = \text{Tr}((WA_\alpha)^\top (WA_\beta)) \\ &= \text{Tr}(A_\alpha^\top W^\top WA_\beta) = \text{Tr}((-A_\alpha) C A_\beta) = -\text{Tr}(A_\alpha C A_\beta), \end{aligned}$$

where we defined the $r \times r$ Gram matrix

$$C := W^\top W \in \mathbb{R}^{r \times r}, \quad C = C^\top \succeq 0.$$

Let

$$C = U\Lambda U^\top, \quad \Lambda = \text{diag}(\lambda_1, \dots, \lambda_r), \quad \lambda_i > 0$$

(on the full-rank set). Since Tr is invariant under orthogonal conjugation, we can compute the spectrum of $G(W)$ in the eigenbasis of C . In that basis, $C = \Lambda$ is diagonal.

Now take the standard orthonormal basis of $\mathfrak{o}(r)$: for $1 \leq i < j \leq r$,

$$A_{ij} := \frac{E_{ij} - E_{ji}}{\sqrt{2}}, \quad A_{ij}^\top = -A_{ij}.$$

Compute the corresponding diagonal entries:

$$\mu_{ij} := \langle WA_{ij}, WA_{ij} \rangle = \text{Tr}(A_{ij}^\top \Lambda A_{ij}) = -\text{Tr}(A_{ij} \Lambda A_{ij}).$$

We evaluate $\text{Tr}(A_{ij} \Lambda A_{ij})$ explicitly. First note the matrix identities (valid for $i \neq j$):

$$\Lambda E_{ij} = \lambda_i E_{ij}, \quad \Lambda E_{ji} = \lambda_j E_{ji}, \quad E_{ij} E_{ji} = E_{ii}, \quad E_{ji} E_{ij} = E_{jj}, \quad E_{ij} E_{ij} = 0 = E_{ji} E_{ji}.$$

Then

$$\begin{aligned} A_{ij} \Lambda A_{ij} &= \frac{1}{2}(E_{ij} - E_{ji})\Lambda(E_{ij} - E_{ji}) \\ &= \frac{1}{2}(E_{ij}\Lambda E_{ij} - E_{ij}\Lambda E_{ji} - E_{ji}\Lambda E_{ij} + E_{ji}\Lambda E_{ji}) \\ &= \frac{1}{2}(\lambda_j E_{ij} E_{ij} - \lambda_j E_{ij} E_{ji} - \lambda_i E_{ji} E_{ij} + \lambda_i E_{ji} E_{ji}) \\ &= \frac{1}{2}(0 - \lambda_j E_{ii} - \lambda_i E_{jj} + 0) = -\frac{1}{2}(\lambda_j E_{ii} + \lambda_i E_{jj}). \end{aligned}$$

Taking the trace gives

$$\text{Tr}(A_{ij} \Lambda A_{ij}) = -\frac{1}{2}(\lambda_i + \lambda_j), \quad \implies \quad \mu_{ij} = \frac{1}{2}(\lambda_i + \lambda_j).$$

In addition, one checks that $\langle WA_{ij}, WA_{k\ell} \rangle = 0$ unless $\{i, j\} = \{k, \ell\}$, so the Gram matrix is diagonal in this basis. Therefore $G(W)$ has eigenvalues

$$\mu_{ij} = \frac{1}{2}(\lambda_i + \lambda_j), \quad 1 \leq i < j \leq r.$$

Log-determinant correction. The log determinant of the orbit Gram matrix is

$$\log \det G(W) = \sum_{1 \leq i < j \leq r} \log(\lambda_i + \lambda_j) + \text{const.}$$

On the full-rank set, take the singular value decomposition

$$W = Q \Sigma R^\top, \quad Q \in \mathbb{R}^{d \times r}, \quad Q^\top Q = I_r, \quad R \in O(r), \quad \Sigma = \text{diag}(\sigma_1, \dots, \sigma_r), \quad \sigma_i > 0.$$

Then

$$C = W^\top W = R \Sigma^2 R^\top, \quad P = W W^\top = Q \Sigma^2 Q^\top.$$

Hence the eigenvalues of C are $\lambda_i = \sigma_i^2$, and the loss depends only on (Q, λ) through $P = Q \Lambda Q^\top$ with $\Lambda = \text{diag}(\lambda_i)$.

To make the PCA structure explicit, define the empirical second moment matrix

$$S := \sum_{x \in \mathcal{B}} x x^\top \in \mathbb{R}^{d \times d}, \quad S = S^\top \succeq 0.$$

Expand the loss:

$$\begin{aligned} \mathcal{L}(W) &= \sum_{x \in \mathcal{B}} \|x - Px\|^2 = \sum_{x \in \mathcal{B}} (x - Px)^\top (x - Px) \\ &= \sum_{x \in \mathcal{B}} (x^\top x - 2x^\top Px + x^\top P^2 x) \\ &= \text{Tr}(S) - 2 \text{Tr}(SP) + \text{Tr}(SP^2), \end{aligned}$$

where we used $x^\top Px = \text{Tr}(Pxx^\top)$ and linearity of trace. Now substitute $P = Q \Lambda Q^\top$ and $P^2 = Q \Lambda^2 Q^\top$:

$$\begin{aligned} \text{Tr}(SP) &= \text{Tr}(SQ\Lambda Q^\top) = \text{Tr}(Q^\top SQ \Lambda) = \sum_{i=1}^r \lambda_i s_i, \\ \text{Tr}(SP^2) &= \text{Tr}(SQ\Lambda^2 Q^\top) = \text{Tr}(Q^\top SQ \Lambda^2) = \sum_{i=1}^r \lambda_i^2 s_i, \end{aligned}$$

where we defined

$$s_i := q_i^\top S q_i \geq 0, \quad q_i \text{ the } i\text{-th column of } Q.$$

Therefore

$$\mathcal{L}(Q, \lambda) = \text{Tr}(S) - \sum_{i=1}^r (2\lambda_i - \lambda_i^2) s_i.$$

When $\sigma^2/\beta = 0$ (no symmetry correction), minimizing $\mathcal{L}(Q, \lambda)$ gives:

- For any i with $s_i > 0$, the scalar map $\lambda \mapsto -(2\lambda - \lambda^2)s_i$ has derivative $2(\lambda - 1)s_i$, so its unique stationary point is $\lambda_i = 1$. Since $2\lambda - \lambda^2 \leq 1$ for all $\lambda \in \mathbb{R}$ with equality at $\lambda = 1$, this stationary point is the minimizer.
- With $\lambda_i = 1$, the loss becomes

$$\mathcal{L}(Q, \lambda \equiv 1) = \text{Tr}(S) - \sum_{i=1}^r s_i = \text{Tr}(S) - \text{Tr}(Q^\top SQ).$$

Thus minimizing \mathcal{L} over Q is equivalent to maximizing $\text{Tr}(Q^\top SQ)$ over $Q^\top Q = I_r$, whose maximizers are given by taking the columns of Q to be the top- r eigenvectors of S . This recovers standard PCA.

When $\sigma^2/\beta \neq 0$, the effective loss is

$$\mathcal{L}_{\text{eff}}(Q, \lambda) = \text{Tr}(S) - \sum_{i=1}^r (2\lambda_i - \lambda_i^2) s_i + \kappa \sum_{1 \leq i < j \leq r} \log(\lambda_i + \lambda_j) + \text{const.}$$

The $\log \det G$ term is independent of Q , so Q is still selected by the PCA part for given λ . We can check how λ is selected by computing the derivative with respect to λ_i :

$$\frac{\partial}{\partial \lambda_i} \left(- \sum_{k=1}^r (2\lambda_k - \lambda_k^2) s_k \right) = 2(\lambda_i - 1)s_i,$$

and

$$\frac{\partial}{\partial \lambda_i} \left(\sum_{a < b} \log(\lambda_a + \lambda_b) \right) = \sum_{j \neq i} \frac{1}{\lambda_i + \lambda_j}.$$

Thus, at an interior critical point with all $\lambda_i > 0$,

$$2(\lambda_i - 1)s_i + \kappa \sum_{j \neq i} \frac{1}{\lambda_i + \lambda_j} = 0, \quad i = 1, \dots, r. \quad (53)$$

This equation has two immediate consequences.

- If $s_i > 0$, then the second term is strictly positive, so $2(\lambda_i - 1)s_i$ must be strictly negative, which forces

$$\lambda_i < 1.$$

So the gauge correction shrinks the singular values away from the exact-projector value $\lambda_i = 1$ preferred by the pure PCA loss.

- If $s_i = 0$, then the loss part does not depend on λ_i , while the gauge derivative remains strictly positive for any $\lambda_i > 0$. So (53) cannot hold in the interior. The minimizer is driven to the boundary $\lambda_i \downarrow 0$. This expresses an effective rank-selection pressure: directions that carry no data variance are suppressed by the orbit-volume term.

The derivation of the orbit Gram determinant assumes $\text{rank}(W) = r$ so that the $O(r)$ action is free and all $\lambda_i > 0$. Equation (53) shows that the gauge term can drive some λ_i toward 0, where the orbit dimension drops and the free-action assumption breaks. This is consistent with the interpretation that the symmetry-induced term favors regions where the orbit metric becomes small, and in the present model this corresponds to approaching lower effective rank.

C Discrete Symmetries

Our focus so far has been on *continuous* parametrization symmetries (\mathcal{G} is a Lie group), where each orbit \mathcal{O}_θ is a smooth manifold, and the noise metric degeneracy induces a gauge correction. We now examine an important class of *discrete* symmetries that play a relevant role in modern neural network architectures, showing that they induce a distinct, combinatorial, entropic bias.

Consider a two-layer neural network with pointwise nonlinearity:

$$f_\theta(x) = W_2 \phi(W_1 x),$$

where $W_1 \in \mathbb{R}^{m \times d}$ and $W_2 \in \mathbb{R}^{k \times m}$. Let $P \in S_m$ be any permutation matrix. Then the reparameterization

$$(W_1, W_2) \mapsto (PW_1, W_2 P^\top)$$

leaves $f_\theta(x)$ unchanged for all x . The group S_m therefore acts by parameterization symmetry:

$$\rho(P, (W_1, W_2)) = (PW_1, W_2P^\top), \quad P \in S_m.$$

The orbit

$$\mathcal{O}_\theta = \{\rho(P, \theta) : P \in S_m\}$$

is a finite set of parameterizations realizing exactly the same model.

Since S_m is finite, the dimension of the orbit is zero; there are no infinitesimal generators and no tangent space. Thus, the gradient noise metric has no degeneracy along the orbit, and *permutation symmetry does not contribute to the gauge term*. In contrast to continuous symmetries, there is no Riemannian volume element to correct.

Combinatorial entropic correction on the quotient Although there is no geometric gauge correction, the discrete symmetry still induces an implicit bias. Let $[\theta]$ denote the equivalence class \mathcal{O}_θ . Since SGD noise distributes probability across all members of the orbit, the induced stationary weight on the quotient Θ/S_m is proportional to the *orbit size*:

$$\pi([\theta]) \propto |\mathcal{O}_\theta| = \frac{|S_m|}{|H(\theta)|},$$

where

$$H(\theta) = \{P \in S_m : \rho(P, \theta) = \theta\}$$

is the stabilizer subgroup of θ . Equivalently, the reduced dynamics includes the *discrete term*

$$L_{\text{discrete}}(\theta) = \frac{1}{\beta} \log |\mathcal{O}_\theta| = \frac{1}{\beta} \log |H(\theta)| + \text{const.} \quad (\text{D1})$$

Thus, configurations with larger stabilizers (i.e. a higher number of internal neuron duplications) have lower energy.

Neuron collapse as implicit bias. If two hidden neurons become identical ($v_i = v_j$ in W_1 and rows i, j identical in W_2), then the permutation swapping them lies in $H(\theta)$. As many neurons collapse to the same parameters, $|H(\theta)|$ grows factorially:

$$W_1(i, :) = W_1(j, :) \quad \forall i, j \quad \Rightarrow \quad |H(\theta)| = m!,$$

minimizing L_{discrete} . Therefore, the implicit bias driven by permutation symmetry and stochasticity in SGD favours *low-distinctness representations*: multiple hidden units degenerate to a single functional unit. This aligns with recent observations of *neuron collapse* and *topological breakdown* phases in wide neural networks trained with large-step or noisy SGD ([30], Figure 5).

In conclusion, we distinguish two sources of entropic implicit bias, both arising solely from *parameterization redundancy*, independent of explicit regularization. The former biases the allocation of the internal representation across layers (e.g. balanced singular-value splits), while the latter biases the *number of distinct functional neurons*.

D Inverse design of implicit bias via symmetry engineering

D.1 Inverse-designed ℓ_1 sparsity

Classically, ℓ_1 penalties such as the LASSO [60] are added explicitly to the loss a model is trained on, in order to induce parameter sparsity – and implicit-bias results for linear models typically point to minimum- ℓ_2 or minimum-nuclear-norm solutions.

Here, we show that a simple factorized parameterization and its induced coordinate-wise gauge symmetry are enough to turn the isotropic stochastic noise of SGD in parameter space into an *implicit* ℓ_1 -minimizing bias on the learned weights.

Model, target bias, and factorized parameterization We start by considering a standard linear regression problem

$$f_w(x) = w^\top x, \quad w \in \mathbb{R}^d,$$

with $n < d$, so that many interpolating solutions w exist. Gradient descent optimization (or SGD in its diffusion limit) on w is known to converge to the minimum- ℓ_2 solution among existing interpolators. Our target bias is instead to induce a LASSO-type implicit penalty on w , i.e.

$$\|w\|_1 = \sum_{i=1}^d |w_i|.$$

To engineer this bias, we introduce the factorized model parameterization

$$w_i = u_i v_i, \quad i = 1, \dots, d,$$

with parameters $(u, v) \in \mathbb{R}^d \times \mathbb{R}^d$, so that

$$f_{u,v}(x) = \sum_{i=1}^d (u_i v_i) x_i = (u \odot v)^\top x.$$

Symmetry group, orbit, and tangent space The parameterization introduced above admits a coordinate-wise gauge symmetry: for each $c = (c_1, \dots, c_d) \in \mathcal{G} = (\mathbb{R} \setminus \{0\})^d$,

$$u_i \mapsto c_i u_i, \quad v_i \mapsto c_i^{-1} v_i, \tag{54}$$

which leaves $w_i = u_i v_i$, and hence f , invariant. Thus, the zero-loss manifold is foliated by

$$\mathcal{O}_{(u,v)} = \{(c \odot u, c^{-1} \odot v) : c \in \mathcal{G}\}.$$

For each coordinate i , consider the one-parameter subgroup $c_i(t) = e^{ta_i}$ with all other $c_j = 1$. Differentiating at $t = 0$ gives the infinitesimal gauge direction

$$\delta u_i = a_i u_i, \quad \delta v_i = -a_i v_i.$$

Absorbing a_i into the generator, a basis vector for the i -th symmetry direction is

$$e_i = (0, \dots, 0, u_i, 0, \dots, 0; 0, \dots, 0, -v_i, 0, \dots, 0), \tag{55}$$

and

$$T_{(u,v)} \mathcal{O}_{(u,v)} = \text{span}\{e_1, \dots, e_d\}.$$

Metric, Gram matrix, and gauge correction We equip $\Theta = \mathbb{R}^{2d}$ with the Euclidean metric

$$\langle (\delta u, \delta v), (\delta u', \delta v') \rangle = \sum_i \delta u_i \delta u'_i + \sum_i \delta v_i \delta v'_i.$$

Under this metric, the basis vectors (55) are orthogonal: $\langle e_i, e_j \rangle = 0$ for $i \neq j$, and

$$\|e_i\|^2 = u_i^2 + v_i^2.$$

Thus, the orbit Gram matrix is diagonal:

$$G_\theta(i, j) = \langle e_i, e_j \rangle = \delta_{ij}(u_i^2 + v_i^2),$$

and its determinant:

$$\det G_\theta = \prod_{i=1}^d (u_i^2 + v_i^2). \quad (56)$$

The gauge correction induced by symmetry is given by:

$$L_{\text{gauge}}(u, v) = \frac{\sigma^2}{2\beta} \sum_{i=1}^d \log(u_i^2 + v_i^2). \quad (57)$$

Eliminating redundancy and ℓ_1 implicit bias On the zero-loss manifold, the effective weights $w_i = u_i v_i$ are fixed by the data; the gauge symmetry explores all pairs (u_i, v_i) with fixed product w_i . As shown in subsection 3.1 for the case of $A = I$, this leads to:

$$\min_{\substack{(u, v): \\ u \odot v = w}} (\|u\|_2^2 + \|v\|_2^2) = 2 \sum_{i=1}^d |w_i| = 2\|w\|_1. \quad (58)$$

Numerical confirmation. To validate the prediction that such factorized parametrization induces an implicit ℓ_1 -type sparsity bias, we consider a synthetic linear regression problem with $d = 200$ features and outputs labeled as $y_{\text{true}} = w_{\text{true}}^\top x$, w_{true} being a sparse ground-truth solution w_{true} having only 1/10th of its entries non-zero by design. We generate an underdetermined training set with $n = 80 < d$ samples, so that many interpolating solutions exist. We then compare two models trained by SGD on the same dataset, driven by the MSE loss: (i) a baseline *vanilla* linear model $f_w(x) = w^\top x$, which is known to select minimum- ℓ_2 solutions; and (ii) our *inverse-designed* model with factorized parametrization $w = u \odot v$ bearing coordinate-wise gauge symmetry. Both models achieve (near) zero training error, but they differ markedly in the structure of the optimized weights: the vanilla model produces a dense solution with large ℓ_1 norm and ultimately poor generalization, whereas the factorized model converges to a much sparser w with substantially smaller ℓ_1 norm and lower test error. Figure 9 quantifies such differences by comparing the evolution of tracked metrics along training.

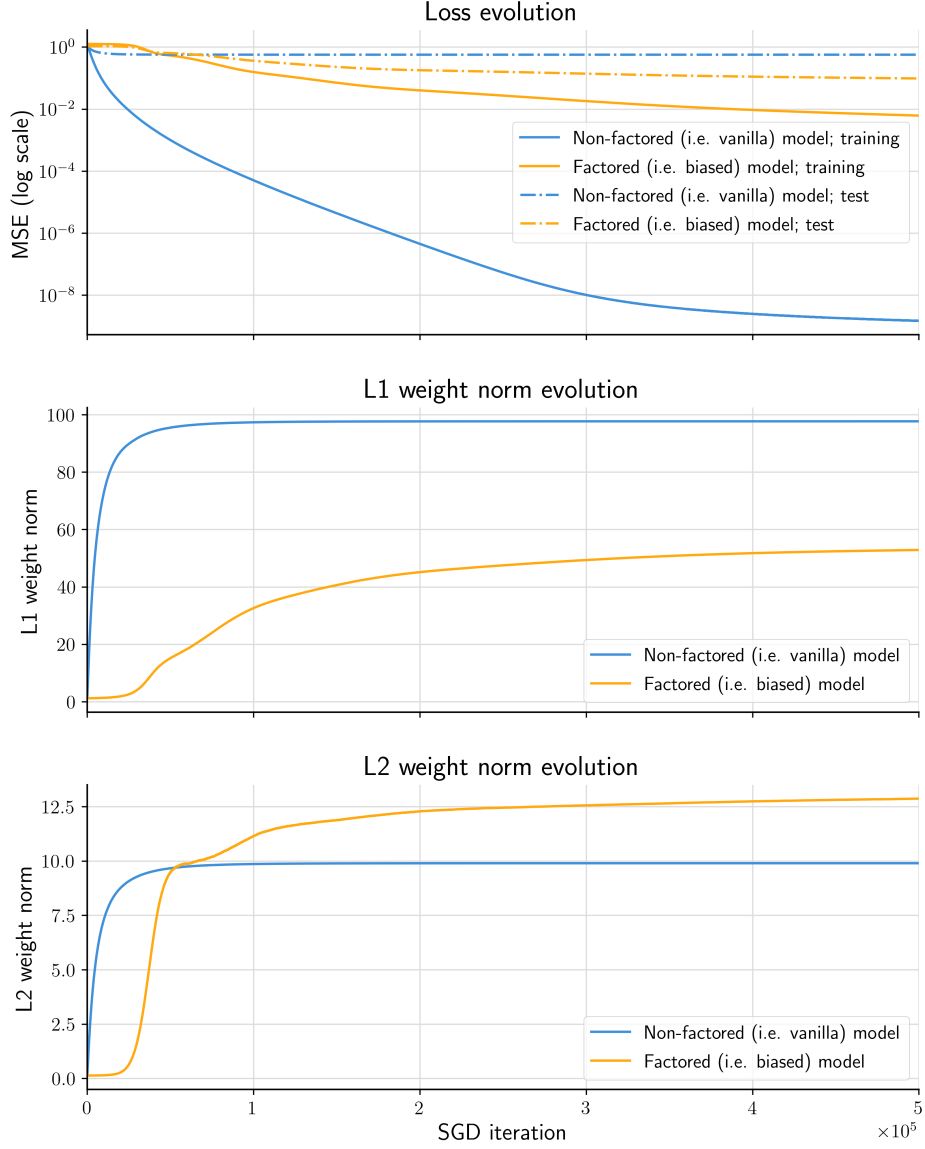


Figure 9: Inverse design of LASSO-like sparsity-producing inductive bias. **Top** As training progresses, the non-biased model achieves near-zero loss over the training set, without significant improvement of the test loss – a clean signal of overfitting. The corresponding biased model experiences a steady improvement in both losses, with its test loss soon overcoming that of the vanilla model – thus attaining far better generalization. **Middle, Bottom** As training progresses, under the effect of no explicit regularization, overall L_1 and L_2 norms of model weights stabilize in magnitude. Weight norms of the biased model ($\|w\|_1 = 53.0$; $\|w\|_2 = 12.9$) attain a much closer match with those of the original *ground truth* data-generating model ($\|w\|_1 = 50.3$; $\|w\|_2 = 14.5$) with respect to the *vanilla* model ($\|w\|_1 = 97.7$; $\|w\|_2 = 10.0$), which exhibits a ridge-like implicit bias.

D.2 Inverse-designed group sparsity (Group LASSO) via block gauge symmetry

Group LASSO penalties $\sum_g \|w_g\|_2$ are standard tools to achieve structured sparsity [61, 62, 63], but are usually imposed explicitly. We now show that a simple blockwise gauge symmetry turns the ℓ_2 geometry in parameter space into an *implicit group-LASSO* bias on the effective weights.

Block parameterization and symmetry Partition $w \in \mathbb{R}^d$ into G disjoint blocks

$$w = (w_1, \dots, w_G), \quad w_g \in \mathbb{R}^{k_g}, \quad \sum_{g=1}^G k_g = d.$$

and introduce the block-wise parameterization

$$w_g = s_g t_g, \quad s_g \in \mathbb{R}, \quad t_g \in \mathbb{R}^{k_g}. \quad (59)$$

The symmetry group is the G -dimensional multiplicative torus

$$\mathcal{G} = (\mathbb{R}_{>0})^G,$$

acting independently on each block as:

$$(s_g, t_g) \mapsto (c_g s_g, c_g^{-1} t_g), \quad c_g > 0. \quad (60)$$

This leaves $w_g = s_g t_g$ (and hence f) invariant. The restriction $c_g > 0$ eliminates a separate discrete sign symmetry that does not contribute to continuous volume.

Symmetry tangents and gauge correction Let $\Theta = \mathbb{R}^G \times \mathbb{R}^d$ have coordinates (s, t) . For block g , the one-parameter subgroup $c_g(\tau) = e^{\tau a_g}$ gives

$$\delta s_g = a_g s_g, \quad \delta t_g = -a_g t_g.$$

A basis generator is therefore

$$e_g = (\dots, 0, s_g, 0, \dots; \dots, 0, -t_g, 0, \dots)$$

supported only on block g . Under the Euclidean noise metric, different blocks are orthogonal and

$$\|e_g\|^2 = s_g^2 + \|t_g\|_2^2, \quad G_\theta(g, h) = \delta_{gh}(s_g^2 + \|t_g\|_2^2).$$

Thus,

$$\det G_\theta = \prod_{g=1}^G (s_g^2 + \|t_g\|_2^2), \quad L_{\text{gauge}}(s, t) = \frac{1}{2\beta} \sum_{g=1}^G \log(s_g^2 + \|t_g\|_2^2) + \text{const.} \quad (61)$$

Minimum-volume representatives and group LASSO On the zero-loss manifold, the effective blocks w_g are fixed. For each block,

$$t_g = \frac{w_g}{s_g}, \quad s_g \neq 0,$$

so that the symmetry-volume factor for block g reduces to the scalar function

$$\phi_g(s_g; w_g) = s_g^2 + \|t_g\|_2^2 = s_g^2 + \frac{\|w_g\|_2^2}{s_g^2}. \quad (62)$$

Let $w_g \neq 0$. Then, we have:

$$\min_{s_g \neq 0} (s_g^2 + \frac{\|w_g\|_2^2}{s_g^2}) = 2\|w_g\|_2.$$

Define $\alpha = s_g^2 > 0$ and $a = \|w_g\|_2^2$. Then, $\phi_g(\alpha) = \alpha + a/\alpha$. Differentiating yields $\phi'_g(\alpha) = 1 - a/\alpha^2$, so the unique critical point is at $\alpha = a^{1/2}$. Convexity for $\alpha > 0$ gives a unique minimum:

$$\phi_g(\alpha^*) = 2a^{1/2} = 2\|w_g\|_2.$$

Summing over blocks and dividing by 2 (as in the standard gauge reduced potential) yields the group LASSO penalty:

$$\min_{\substack{(s,t): \\ s_g t_g = w_g}} \frac{1}{2} (\|s\|_2^2 + \|t\|_2^2) = \sum_{g=1}^G \|w_g\|_2. \quad (63)$$

Emergence of structured sparsity Blocks with small $\|w_g\|_2$ permit large symmetry volume (large $\det G_\theta$), which is penalized by the gauge correction (61). Hence SGD implicitly *minimizes the effect of entire blocks* by pushing such vectors exactly to zero.

Numerical validation. We validate such theoretical prediction on a synthetic group-sparse regression task. The input dimension is still chosen to be $d = 200$, randomly partitioned into $G = 40$ non-overlapping groups of size 5. Only 5 groups are active in the ground-truth solution w^* used to label the inputs as $y_{\text{true}} = w_{\text{true}}^\top x$. We then compare two models trained by SGD on the same dataset, driven by MSE loss: (i) a standard linear model $f(x) = w^\top x$, with no regularization; (ii) the block-rank-one factorization (59) trained in (s, t) , which possesses the blockwise gauge symmetry. Both models achieve near-zero training error; however, while both achieve comparable MSE also on validation dataset, their respective implicit biases differ markedly. As predicted by (63), the factorized model drives most blocks toward zero, making them inactive and minimizing the group-LASSO potential $\sum_g \|w_g\|_2$, whereas the vanilla model does not and converges to a dense solution. Figure 10 represents such difference, by tracking the relevant metrics as training progresses.

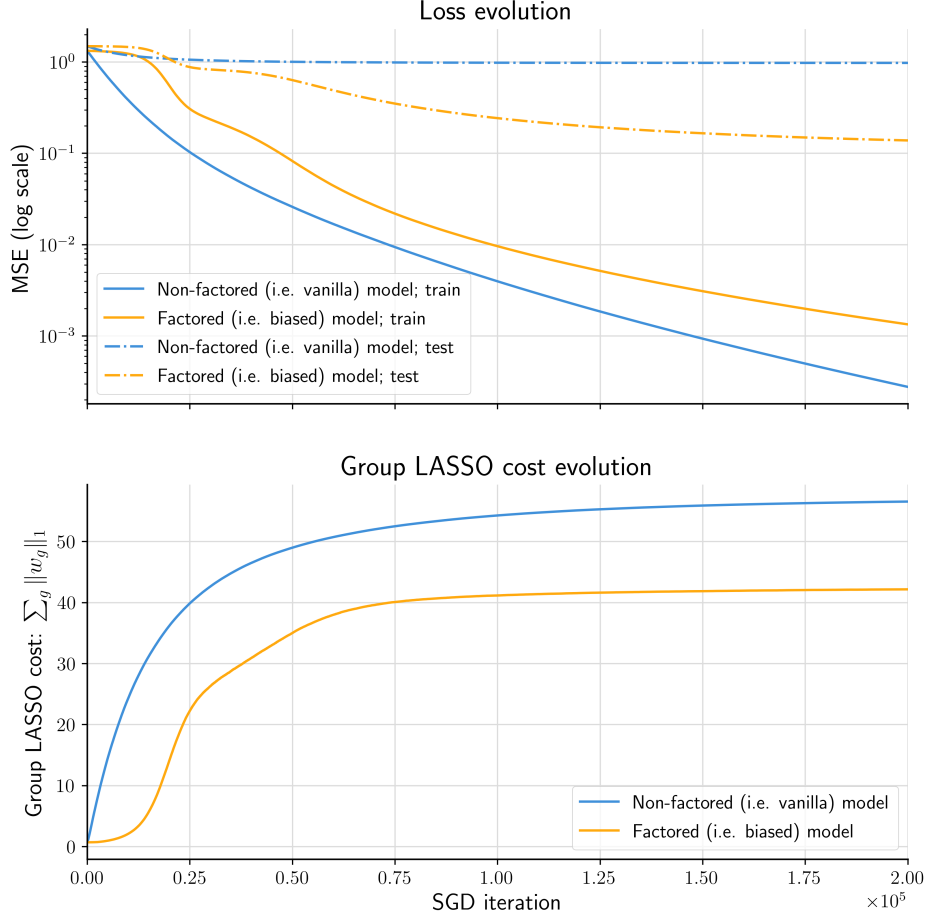


Figure 10: Inverse design of group LASSO-like sparsity-producing inductive bias. **Top** As training progresses, the non-biased model fails to achieve significant improvement in its loss over the test-set, while its training loss decreases – a clean signal of overfitting. The biased model instead experiences a steady improvement in both losses, with its test loss soon overcoming that of the vanilla model – thus attaining far better generalization. **Bottom** As training progresses, under the effect of no explicit regularization, the group LASSO cost for the weights of both models stabilize in magnitude. The biased model ($\|w\|_1 = 81.4$; $\|w\|_2 = 14.2$) achieves better adherence to overall weight norm statistics of the original *ground truth* data-generating model ($\|w\|_1 = 72.3$; $\|w\|_2 = 17.3$) with respect to the *vanilla* model ($\|w\|_1 = 106.0$; $\|w\|_2 = 9.89$). The same can be said about parameter groups exhibiting a group norm higher than a given threshold (0.2 in our case): 55% for the biased model; 100% for the *vanilla* model; with a ground truth of 12.5%.

E Proofs of mathematical results in the main text

E.1 Proof of Theorem 1

Proof. For readability, we set $\beta = 1$ and $\sigma^2 = 1$. Restoring the original values of (β, σ^2) is deferred to the rescaling shown at the end.

By assumption,

$$\mu_\infty(d\theta) = Z^{-1} e^{-L(\theta)} d\text{Vol}_\Theta(\theta).$$

We want to compute the conditional law of μ_∞ on the slice $\mathcal{S} = \chi^{-1}(0)$. A standard way to represent

this conditional law is to *constrain the (unnormalized) measure*

$$\Omega_{\mathcal{S}}(d\theta) := e^{-L(\theta)} \delta^{(m)}(\chi(\theta)) d\text{Vol}_{\Theta}(\theta), \quad (64)$$

where $\delta^{(m)}$ is the m -dimensional Dirac delta on \mathbb{R}^m .

Since χ is a submersion, $\mathcal{S} = \chi^{-1}(0)$ is a smooth embedded submanifold of codimension m . For any integrable function $f : \Theta \rightarrow \mathbb{R}$, we define a constraint identity such as

$$\int_{\Theta} f(\theta) \delta^{(m)}(\chi(\theta)) d\text{Vol}_{\Theta}(\theta) = \int_{\mathcal{S}} f(\theta) \frac{1}{\sqrt{\det G_{\chi}(\theta)}} d\text{Vol}_{\mathcal{S}}(\theta), \quad (65)$$

where

$$(G_{\chi}(\theta))_{ij} = g_{\theta}(\nabla \chi^i(\theta), \nabla \chi^j(\theta)).$$

Let $\varphi : \mathcal{S} \rightarrow \mathbb{R}$ be bounded and measurable. Extend φ to a neighbourhood of \mathcal{S} in Θ (any extension works because the delta enforces $\chi(\theta) = 0$). Apply (65) with

$$f(\theta) = \varphi(\theta) e^{-L(\theta)}.$$

Then

$$\int_{\Theta} \varphi(\theta) e^{-L(\theta)} \delta^{(m)}(\chi(\theta)) d\text{Vol}_{\Theta}(\theta) = \int_{\mathcal{S}} \varphi(\theta) e^{-L(\theta)} \frac{1}{\sqrt{\det G_{\chi}(\theta)}} d\text{Vol}_{\mathcal{S}}(\theta). \quad (66)$$

In particular, taking $\varphi \equiv 1$ gives the normalizing constant for the constrained measure:

$$Z_{\mathcal{S}} := \int_{\mathcal{S}} e^{-L(\theta)} \frac{1}{\sqrt{\det G_{\chi}(\theta)}} d\text{Vol}_{\mathcal{S}}(\theta). \quad (67)$$

Define the probability measure on \mathcal{S} by

$$\mu_{\mathcal{S}}(d\theta) := Z_{\mathcal{S}}^{-1} e^{-L(\theta)} \frac{1}{\sqrt{\det G_{\chi}(\theta)}} d\text{Vol}_{\mathcal{S}}(\theta). \quad (68)$$

Then (66) becomes

$$\int_{\mathcal{S}} \varphi(\theta) \mu_{\mathcal{S}}(d\theta) = \frac{1}{Z_{\mathcal{S}}} \int_{\mathcal{S}} \varphi(\theta) e^{-L(\theta)} \frac{1}{\sqrt{\det G_{\chi}(\theta)}} d\text{Vol}_{\mathcal{S}}(\theta),$$

so $\mu_{\mathcal{S}}$ is absolutely continuous with respect to $d\text{Vol}_{\mathcal{S}}$ and has density

$$\rho_{\mathcal{S}}(\theta) \propto e^{-L(\theta)} \frac{1}{\sqrt{\det G_{\chi}(\theta)}}, \quad \theta \in \mathcal{S}.$$

Starting from (4) with general (β, σ^2) , the same steps apply with the replacement $L(\theta) \mapsto (\beta/\sigma^2)L(\theta)$. Therefore

$$\rho_{\mathcal{S}}(\theta) \propto \exp\left(-\frac{\beta}{\sigma^2} L(\theta)\right) \frac{1}{\sqrt{\det G_{\chi}(\theta)}}, \quad \theta \in \mathcal{S},$$

which gives (6). The equivalent effective-loss form (7) follows from $1/\sqrt{\det G_{\chi}} = \exp\left(-\frac{1}{2} \log \det G_{\chi}\right)$. \square

E.2 Proof of Proposition 1

Proof. Since $\mathcal{S} = \chi^{-1}(0)$, we have $T_\theta \mathcal{S} = \ker d\chi_\theta$. Thus, each $\nabla \chi^i(\theta)$ is orthogonal to $T_\theta \mathcal{S}$, hence $\nabla \chi^i(\theta) \in (T_\theta \mathcal{S})^\perp$. Under the orthogonal-slice assumption, $(T_\theta \mathcal{S})^\perp = \text{span}\{\xi_a(\theta)\}$, so there exists a matrix $\phi(\theta)$ such that

$$\nabla \chi^i(\theta) = \sum_a \phi_{ia}(\theta) \xi_a(\theta).$$

Using $d\chi^i(v) = g(\nabla \chi^i, v)$ and taking $v = \xi_b$ gives

$$M_{ib} = d\chi^i(\xi_b) = g(\nabla \chi^i, \xi_b) = \sum_a \phi_{ia} g(\xi_a, \xi_b) = \sum_a \phi_{ia} H_{ab},$$

and hence $M = \phi H$ and $\phi = MH^{-1}$. Finally,

$$(G_\chi)_{ij} = g(\nabla \chi^i, \nabla \chi^j) = \sum_{a,b} \phi_{ia} \phi_{jb} g(\xi_a, \xi_b) = (\phi H \phi^\top)_{ij}$$

and substituting $\phi = MH^{-1}$ yields $G_\chi = MH^{-1}M^\top$. \square